Cosmic muons in the L3 detector

Diplomarbeit
zur Erlangung des akademischen Grades
Diplom–Physiker

eingereicht von

Andreas Korn
geb. am 22.09.1972 in Berlin

Humboldt-Universität zu Berlin
Mathematisch-Naturwissenschaftliche Fakultät I
Institut für Physik

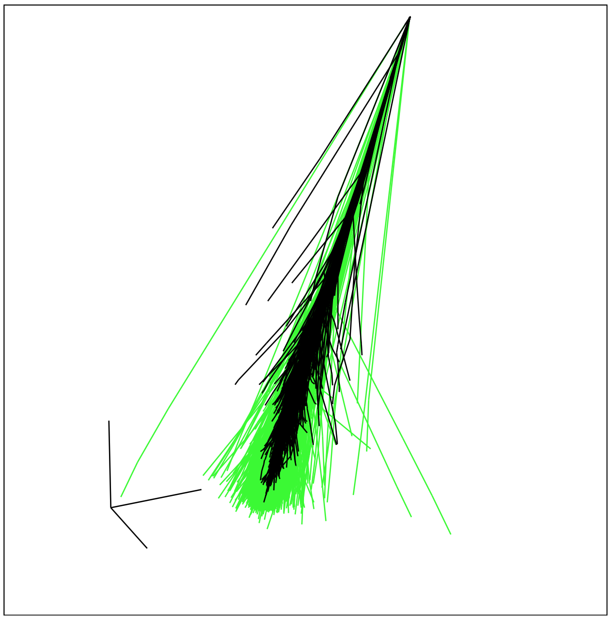

Betreuer: Prof. Th. Hebbeker
Gutachter:
Berlin, 17. Juli 1998

Zusammenfassung

Das L3+Cosmics Experiment ist eine Erweiterung des L3 Detektors. Dieser Detektor befindet sich unter der Erde in einer Tiefe von 52 m am LEP–Beschleunigerring des Forschungslabors CERN in Genf.

Im Rahmen des L3+Cosmics Experiments wird das große Magnetspektrometer des Detektors benutzt, um kosmische Myonen zu vermessen. Dieses Spektrometer besitzt ein Volumen von circa 1000 m^3 und erreicht eine Impulsauflösung von 2.5% für 45 GeV Myonen. Diese Eigenschaften ermöglichen im Vergleich zu vorangegangenen Experimenten eine um den Faktor 10 präzisere Messung des Myonenspektrums.

Ein zusätzlicher Detektor ist nötig, um die Ankunftszeit der Teilchen zu messen. Dieser Detektor besteht aus Szintillationszählern, die über dem Magneten angebracht sind.

Die Installation wird in zwei Schritten vollzogen. In der ersten Phase werden Szintillatoren mit 48m^2 und später 72m^2 im oberen Bereich installiert. Das Experiment startet in Phase I mit einem Viertel des Spektrometers. Für Phase II wird die Szintillatorfläche um den Faktor drei weiter vergrößert und das gesamte Spektrometer genutzt.

Kosmische Myonen entstehen in Schauern, die durch die Wechselwirkung hochenergetischer Teilchen der primären kosmischen Strahlung in der Atmosphäre verursacht werden. Die Untersuchung dieser Myonen erlaubt es die zugrundeliegenden Wechselwirkungsprozesse zu studieren.

In dieser Arbeit ist die Simulation des L3+Cosmics Experimentes beschrieben. Es werden Programme zur Generierung von Myonen, zur Simulation von Luftschauern, für den Transport durch die darüberliegende Erdschicht und zur Ereignis-simulation vorgestellt.

Ein mit diesen Programmen gewonnenes Resultat ist die Akzeptanz. Das Experiment weist in Phase I eine effektive Fläche von $2.67 \pm 0.08\,\mathrm{m}^2$ auf. Diese Fläche erhöht sich auf $42.4 \pm 0.7\,\mathrm{m}^2$ für Phase II. Die Untersuchung von Multi–Myon–Ereignissen ermöglicht es, die Zusammensetzung der primären kosmischen Strahlung zu messen.

Abstract

The L3+Cosmics experiment is an extension of the L3 detector. This detector is situated at the LEP accelerator ring at CERN in Geneva. It is located underground at 52 m depth.

The large magnetic spectrometer is used to measure cosmic muons.

This spectrometer has a volume of 1000m^3 and achieves a resolution of 2.5 % for 45 GeV muons. This properties allow a precision which is a factor of ten better than previous experiments of the muon spectrum. An additional detector is needed to obtain the arrival time of the particles. This detector consist of scintillation counters placed on top of the magnet.

The installation will take place in two steps. In the first phase a scintillator area of 48m^2 and later 72m^2 is installed on top of the magnets. The experiment starts in phase I with a quarter of the spectrometer.

Phase II extends the scintillator coverage to three times the final area of phase I. The full spectrometer is used for phase II.

Cosmic muons originate in air showers. The showers are induced by cosmic primary particles in interactions with the atmosphere. Analysing these muons allows to study the underlying interaction processes.

In this work the simulation of the L3+Cosmics experiment is described. Programs for muon generation, air shower simulation, tracking through the earth layer above the detector and simulating events in the apparatus are introduced.

A result obtained with these programs is the acceptance. Phase I of the experiment corresponds to an effective area of $2.67 \pm 0.08\,\text{m}^2$. This increases to $42.4 \pm 0.7\,\text{m}^2$ for phase II. Studies of multi muons indicate a possibility to measure the primary composition of cosmic rays.

Contents

Chapter 1

Introduction

1.1 Motivation

The branch of astro particle physics emerged from elementary particle physics and astronomy. It explores the structure of the universe at the smallest and largest possible scales at once. The main subject of astro particle physics is the investigation of cosmic rays. Although it has been under study for nearly a century, the cosmic radiation is still a topic of great interest.

For particle physicists cosmic rays remain the source of the most energetic particles available. They provide the possibility to search for new physics phenomena in regions which will become accessible at accelerators only in decades.

For astronomers cosmic rays open a window to study high energy processes in the universe. If we include also the visible light into this category, cosmic radiation is the only information we get from objects outside our solar system.

1.2 A short history of astro particle physics

The first evidence for an extraterrestrial ionising radiation came from an experiment by T.Wulf in 1910. Wulf's measurement at the top of the Eiffel tower revealed an ionisation that was too strong to be explained by natural radioactivity alone.

Two years later, in 1912, V.Hess made ionisation measurements during several balloon flights [1]. He showed that above 1.5 km the intensity of the radiation increased with increasing altitude. This was the discovery of cosmic rays. Millikan was the first to assign this name [2]. Bothe and Kolhörster showed that these rays consist mainly of charged particles. They used for the first time a coincidence technique [3]. A gold absorber was placed between two Geiger–Müller counters, which had just been invented. Simultaneous signals in both tubes proved the penetrating power of the traversing particles. Observations of Skobelzyn suggested that these particles were produced in showers [4].

After the particle nature of cosmic rays was established a number of new particles were discovered. The existence of the positron was established by Anderson [5]. This confirmed Dirac's prediction of antiparticles. The muon was discovered in 1937 by Anderson and Neddermeyer at Caltech [6]. The pion, predicted by Yukawa as exchange particle of the nuclear force, was found in 1947. Lattes, Powell and Occhialini investigated tracks in a photographic emulsion. They found a two step decay of a particle with a mass between that of an electron and a proton [7]. These tracks were interpreted as the decay of a pion into a muon, which then decayed further into an electron.

The first decays of strange particles were seen in the same year. These so called V–events supported an early observation of a particle, today known as K^+, in collisions [8]. The two decay modes of this particle into two or three pions were for a long time attributed to two different particles. The two pions form a state of even parity. The three pion configuration has odd parity. Only the equal masses of the parent states suggested that the same particle was involved in both decays. This Θ-τ–puzzle lead eventually to Lee and Yang's hypothesis of parity non-conservation in 1956.

In 1952 the accelerator COSMOTRON started operation at Brookhaven. With this machine cosmic energies were available in artificial particle collisions. From that point accelerator experiments played the leading role for discoveries in particle physics. The research in cosmic ray physics switched to the topic of origin and acceleration. The pioneering work was done by Fermi [9]. The problem remains still unsolved.

The first step to connect cosmic ray and astrophysics was made by Shklovsky in 1952. He suggested that synchrotron emission from high–energy electrons could explain the radio and optical properties of the supernova remnant in the Crab Nebula [10]. With the discovery of Quasars by Schmidt [11] in 1962 the first source candidates came into sight. Another possible source, the pulsars, were discovered in 1967 by Hewish and Bell. In recent years experimental evidence for the acceleration of particles up to hundred TeV in super nova remnants was established [12][13].

1.3 Properties of cosmic rays

1.3.1 Primary spectra

Primary cosmic rays arriving at the top of the atmosphere consist to about 85% of protons. Other components are helium (12%) and heavier nuclei (1%). Electrons and positrons account for the remaining two percent. Gamma rays are also present, but are usually not counted as particle component. They are less frequent than nuclei (0.1%).

The elemental abundance in cosmic rays is very similar to that of the solar

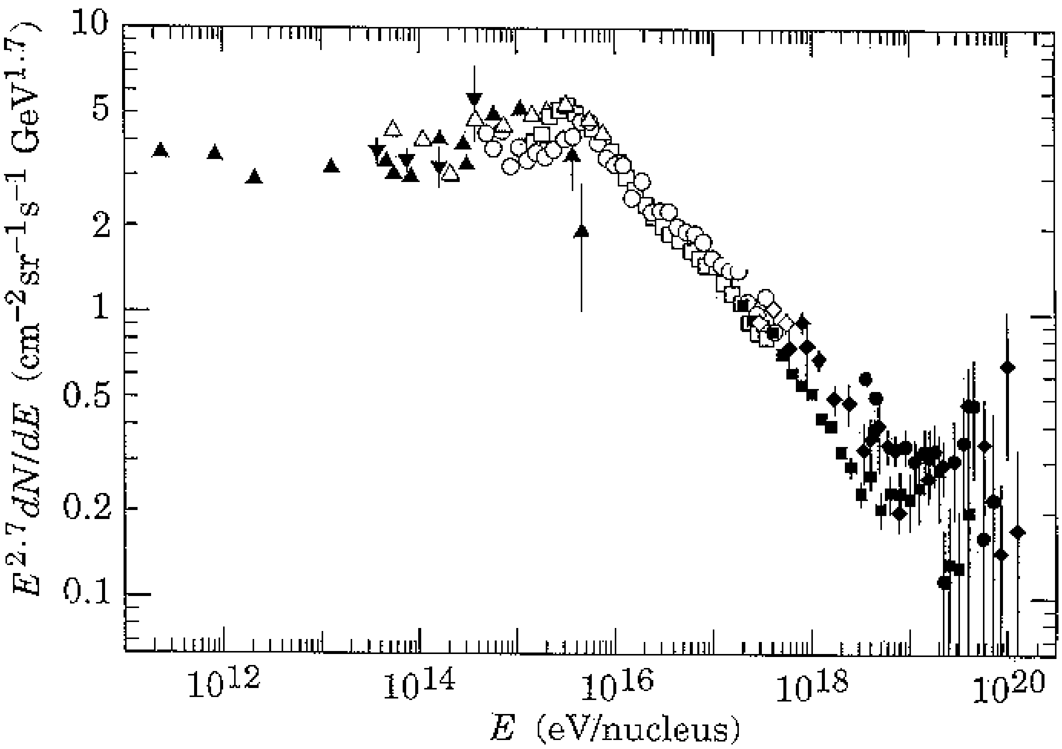

Figure 1.1: Energy distribution of primary cosmic rays. The spectrum is multiplied by $E^{2.7}$ [14].

system. The fact that lithium, beryllium, boron and some heavier nuclei are more abundant in cosmic rays can be explained as a result of spallation [15].

The energy spectrum follows a power law. The exponent lies in the range 2.5–2.7. The spectrum attenuates below 1 GeV due to deflection of particles in magnetic deformations produced by the solar wind. In the high energy region the spectrum shows two distinct features. The exponent of the power law distribution increases around $10^{15} - 10^{16}$ eV, the 'knee' region, and decreases above 10^{19} eV at the so called 'ankle'. The energy dependence of the composition is very badly known. Above the knee no reliable data exist. In the region above 10^{19} eV exists a theoretical cut off due to pion production in interactions with the microwave background. This effect is known as Greisen-Zatsespin-Kuzmin cut off.

1.3.2 Air showers

An extensive air shower is initiated by the interaction of an incident primary particle with a nucleus of the atmosphere. These first interactions takes place at roughly 20 km height. Heavy nuclei have a shorter mean free path and interact earlier as protons. So protons penetrate deeper into the atmosphere.

In this first interaction a number of hadrons is produced. These hadrons consist mainly of pions (about 70 %), but also kaons and charm particles. The ratio of pions to heavier particles depends on energy. The importance of kaons for example increases with energy. The created hadrons interact further with the atmosphere and induce a hadronic cascade.

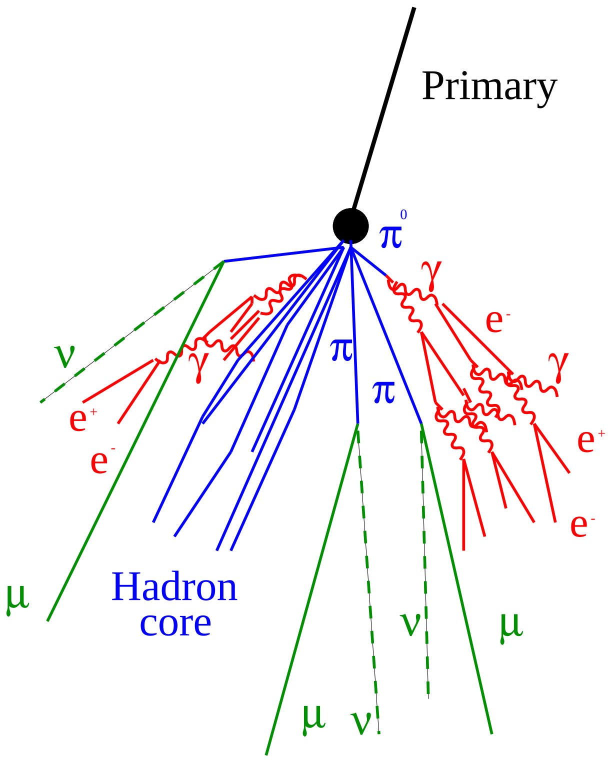

Figure 1.2: Schematic view of a developing air shower.

Neutral pions have a very short life time ($\tau = 8 \cdot 10^{-17}$s). They decay into photons $\pi^0 \to 2\gamma$ and start the development of electromagnetic cascades. The gamma rays produce electron–positron pairs, which in turn radiate photons via bremsstrahlung.

Muons originate from meson decay:

$$\pi^{\pm} \quad \rightarrow \quad \mu^{\pm} + \nu_{\mu}(\bar{\nu_{\mu}}) \tag{1.1}$$
$$K^{\pm} \quad \rightarrow \quad \mu^{\pm} + \nu_{\mu}(\bar{\nu_{\mu}}) \tag{1.2}$$
$$K^{\pm} \quad \rightarrow \quad \pi^0 + \mu^{\pm} + \nu_{\mu}(\bar{\nu_{\mu}}) \tag{1.3}$$

The material of the atmosphere amounts to roughly 30 radiation or 10 interaction lengths. After a number of interactions the remaining energy per particle is too small to produce new secondaries. The shower attenuates. The few remaining hadrons and nuclear fragments form the hadron core. The hadrons are collimated to about 10 m around the shower axis. At surface level a shower consists of about 90 % electrons, positrons and photons, 9 % muons and less than 0.1 % hadrons.

1.3.3 Cosmic muons

Muons are produced by decaying mesons. It is very unlikely for a muon to undergo nuclear interactions. Muons lose energy more or less only by ionisation. That means muons are very penetrating particles and reach the earth surface even from great heights in the atmosphere.

Muons decay within $\tau = 2.2 \cdot 10^{-6}$s. This lifetime is enhanced by relativistic time dilatation. So that muons with an energy above 3 GeV can travel more than 20 km and can originate from the height of first interactions.

At energies below 100 GeV energy loss and absorption are important and the flux varies with the zenith angle θ like [16]:

$$I_\mu(\theta) = \frac{dN}{d\cos\theta} \sim \cos^2\theta.$$

The zenith angle is measured between the perpendicular downward direction and the direction of the particle. At higher energies decay and interaction of the parent meson are competing processes. For larger zenith angles mesons travel larger distances in thin regions of the atmosphere, so that the decay is favoured and the flux varies like:

$$I_\mu(\theta) = \frac{dN}{d\cos\theta} \sim \frac{1}{\cos\theta}$$

In addition muons originating from prompt decaying heavy mesons become increasingly important. Muons from such mesons are isotropically distributed.

In the range from 50 GeV-5 TeV the flux can be well approximated by:

$$\frac{dN_\mu}{dE_\mu} = \frac{0.14}{cm^2 sr GeV} \left(\frac{E_\mu}{GeV}\right)^{-2.7} \left\{ \frac{1}{1 + \frac{1.1 E_\mu \cos\theta}{115 GeV}} + \frac{0.054}{1 + \frac{1.1 E_\mu \cos\theta}{850 GeV}} \right\} \tag{1.4}$$

Here the first term is due to pions and the second arises from kaons [17]. Prompt muons are neglected.

1.4 The L3 detector as tool for cosmic muons

The L3 detector is situated at CERN in Geneva. This apparatus has originally been build to study e^+e collisions. The muon chambers of the L3 detector form the largest magnetic spectrometer available. The momentum resolution is 2.5% at 45 GeV. Together with an excellent angular resolution of 0.1 mrad this will allow a wide range of physics topics to be studied [18]. The main physics goals of the L3+Cosmics project are:

- precise measurement of the differential muon spectrum and its angular dependence in the range 20 to 2000 GeV
- determination of the muon charge ratio as function of energy
- recording of multi muon events
- observation of the moon shadow
- search for coincident events at large scale
- search for exotic events

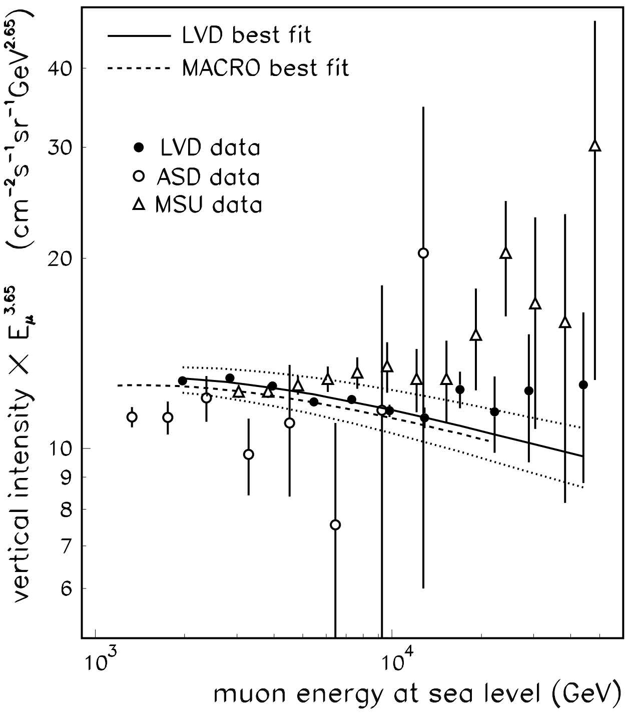

Figure 1.3: Deep underground measurements of the high energy muon spectrum [19].

muon spectrum: Current measurements of the muon spectrum can be divided into 3 categories:

- direct absolute measurements with ground based spectrometers
- unnormalised measurements at shallow depth

- indirect measurements by deep underground experiments using a depth–intensity relation

The L3+Cosmics experiment lies between the first two categories. It is situated under an earth layer of well known composition. A normalisation is still possible as some muons arrive unshielded through an access shaft.

Compared with other spectrometers L3+Cosmics has a larger geometrical acceptance and a wider momentum range. Measurements in the TeV region are mainly indirect measurements which suffer from uncertainties in the energy loss calculation. The angular dependence of high energetic muons has only been measured precisely in the near horizontal direction so far.

The muon flux is related to the flux of muon neutrinos. Both are produced simultaneously. A precise measurement could be used as input in model calculations to reduce the theoretical uncertainty in the atmospheric neutrino flux. This could improve the understanding of recent evidence for neutrino oscillation presented by the Super–Kamiokande Collaboration [20]. Neutrino flux calculations have uncertainties around 20%. This could be reduced by a factor of four.

The angular distribution of muons is sensitive to hadronic interactions in the atmosphere, especially the produced fraction of heavier mesons.

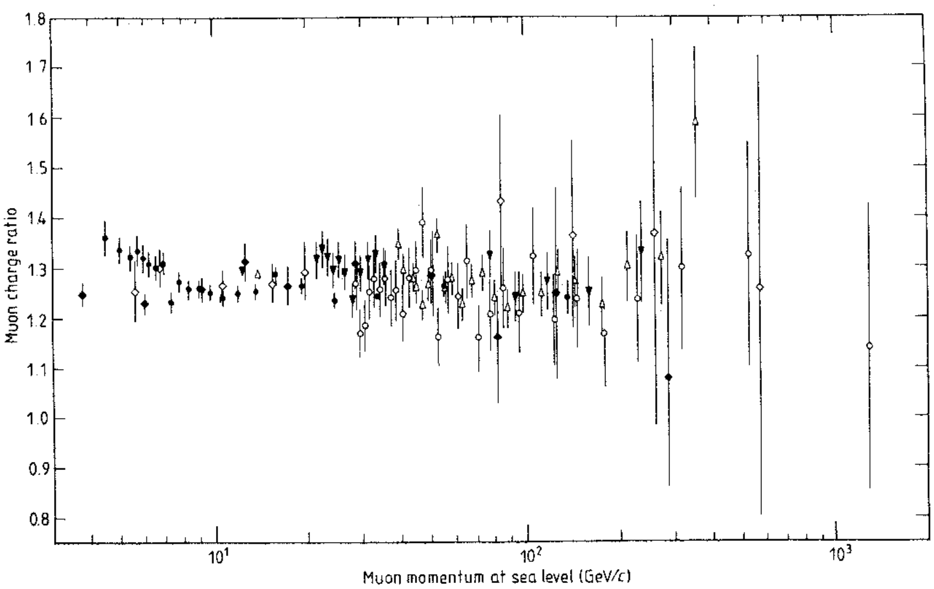

Figure 1.4: Current measurements of the muon charge ratio as function of energy [21].

muon charge ratio As momentum measurements at high energy rely mostly on depth-intensity relations they can make no statement on the charge ratio. The

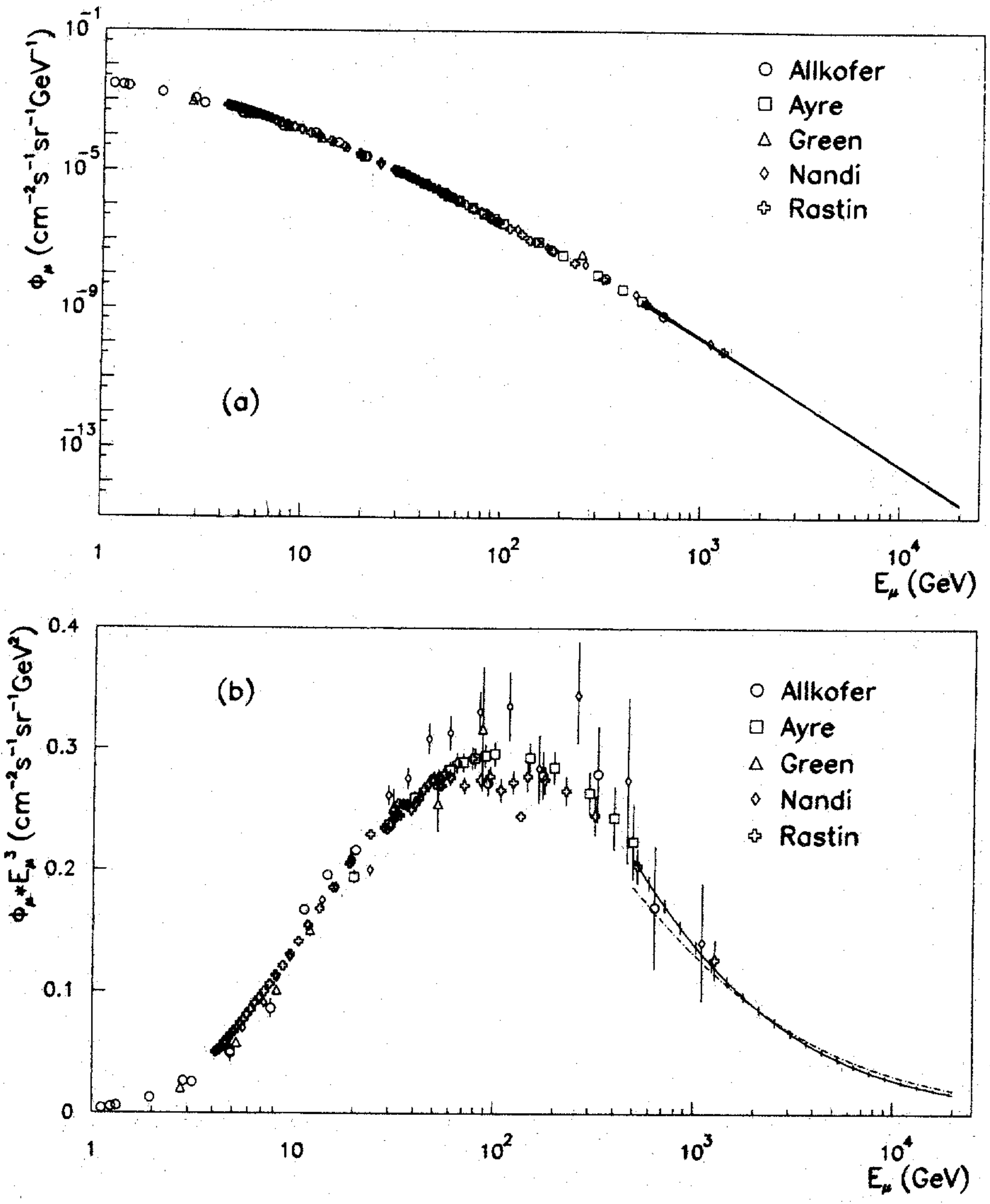

Figure 1.5: Measurements of the muon spectrum. Taken from [22].

experimental situation is bad, as shown in figure 1.4.

The charge ratio is sensitive to the primary composition. It is influenced by the ratio of neutrons to protons in incident nuclei. Nuclear interaction models can also be tested. For example the K/π ratio is important for the charge ratio. The ratio $\frac{K^+}{K^-}$ is greater than $\frac{\pi^+}{\pi^-}$ because negative kaons are suppressed.

multi muon events The muon multiplicity is sensitive to primary composition. This topic is treated in more detail in section 6.4.

moon shadow Primary particles arriving in the moon direction are blocked and do not reach the earth's atmosphere. This effect has been verified by several experiments [23][24][25]. The observation of the moon shadow is a good test of experimental pointing accuracy. As charged particles are deflected in the magnetic field of the earth two separate shadows exist for positive and negative particles. This could be used to set limits on the anti proton flux.

coincident events at large scale In a pioneering experiment detectors at Geneva and Basel separated by 180 km have observed an excess of coincidences [26]. Coincidences at this scale could be explained by interactions of primary cosmic rays in outer sections of the sun [27]. More data are needed to investigate this phenomenon.

exotic events Cosmic ray experiments revealed several events which can not be explained with the present knowledge of physics. Famous examples are the Kolar events. Upgoing tracks with large opening angle have been observed at the Kolar Goldfield Mine. These events have recently been interpreted as the decay of heavy weakly interacting particles (WIMP's) [28]. Such particles are predicted by super symmetric theories.

Chapter 2

L3+Cosmics Detector

The L3+Cosmics setup is an extension of the existing L3 detector [29]. This apparatus is a general purpose detector at LEP. The **L**arge **E**lectron **P**ositron collider is a particle accelerator located at CERN in Geneva. LEP has eight potential collision points. At four of these regions the electron and positron beams are electrostatically separated. The experiments ALEPH, DELPHI, OPAL and L3 are placed at the remaining interaction points. It is planned to use the other LEP detectors also for cosmic ray research. This project is named COSMOLEP [30]. Due to the wide separation this constellation is ideally suited to investigate large coincident events [26]. The first working experiment is COSMOALEPH [31].

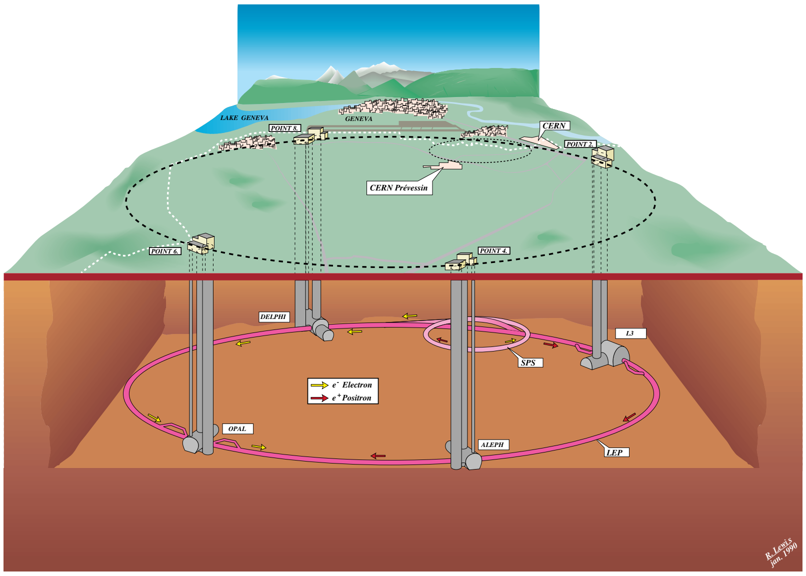

Figure 2.1: .

2.1 L3 Detector

L3 is situated at point 2 of the LEP ring in a hall under 30 m of molasse. Point 2 is located 6^o east and 46^o north. The surface is 470m above sea level. The interaction vertex in the middle of the detector forms the coordinate system origin. The origin is located 44 m underneath surface. The z–direction follows the electron beam. The x–coordinate is directed inwards to the centre of the collider ring. The y–coordinate points upwards. The experiment is on a slope of 1.39 % along the z–axis.

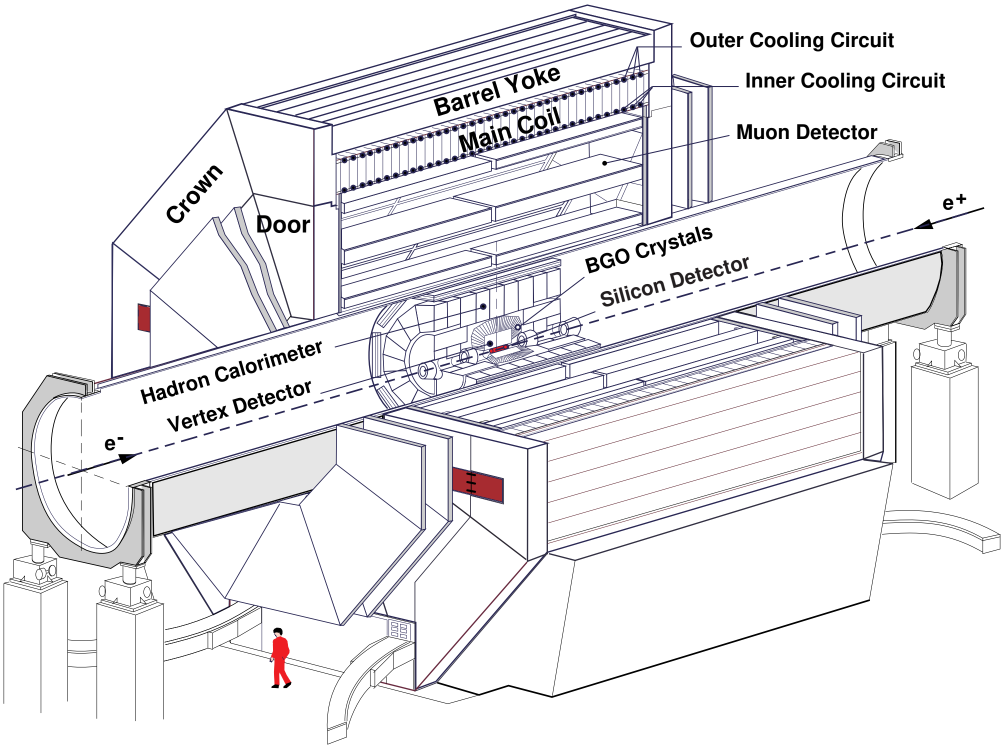

Figure 2.2: Schematic view of the L3 detector.

The L3 detector has a cylindrical structure. The first detector counting from the nominal vertex is the silicon micro vertex detector (SMD). This detector is mounted close to the beam-pipe. It is followed by a time expansion chamber (TEC) used for inner tracking. The next element is the electromagnetic calorimeter formed by 10752 bismuth germanate (BGO) crystals. The BGO barrel is surrounded by scintillation counters. A hadron calorimeter follows. It consists of uranium absorbers and gas wire proportional chambers. The last of the inner detectors is the muon filter. These components are completed in the forward region by a forward tracking chamber (FTC), scintillator endcaps and hadron calorimeter endcaps.

A muon looses about 4 GeV travelling through the inner detector components. All inner parts are installed inside a support tube of 4.45 m diameter. The muon spectrometer is build around this tube. The iron return yoke of the magnet closes the detector. All subdetectors operate in a magnetic field of 0.5 Tesla.

For L3+Cosmics only the barrel muon chambers are used. An additional T0 detector is placed on top of the magnets. These components will be described in some detail in the following sections.

2.2 Muon spectrometer

The muon spectrometer consists of two so called ferris wheels. A ferris wheel is subdivided in eight octants. Each octant is composed of five precision drift chambers (P–chambers) organised in three layers. These chambers measure the track position in the $r\phi$-plane and are used to determine the momentum. The P–chambers are filled with 61.5% Argon and 38.5% Ethane as drift gas.

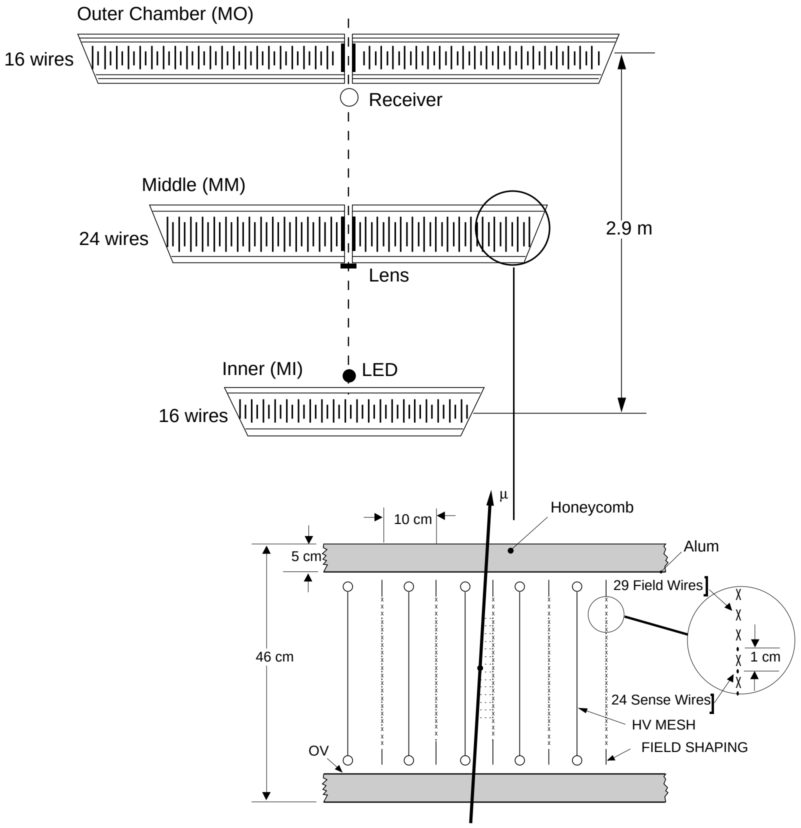

Figure 2.3: One octant of the muon spectrometer.

Inner (MI) and outer (MO) chamber are covered on top and bottom by two staggered z–chambers. A gas mixture of 91.5% Argon and 8.5% Methane is used.

The spectrometer is situated in a solenoidal magnetic field along the beam axis of 0.5 Tesla. The barrel muon system covers 76 % of the solid angle. Forward backward chambers installed in 1994 are not used for L3+Cosmics.

The drift chambers can be subdivided into drift cells. A P–chamber drift cell is formed by a group of sense wires enclosed between two planes of mesh wires. Two cathode mesh planes are 101.50 mm apart. The distance between two sense wires is 9 mm. Additional field wires placed between neighboured sense wires ensure an uniform electrical field of 1100 V/cm. The drift velocity has been measured to a value of $48.6 \pm 5 \mu$m/ns [32].

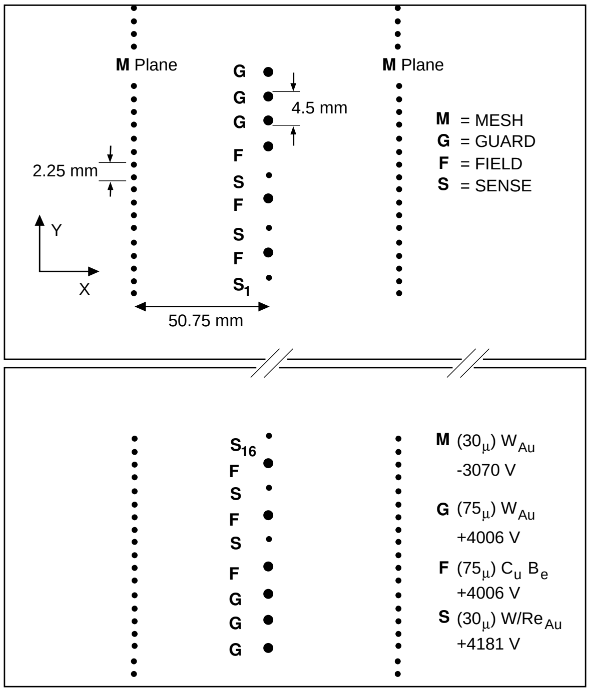

Figure 2.4: The configuration of a P–chamber drift cell in the MO(MI) layer. Only 16 sense wires ($S_1 \cdot S_{16}$) are connected. The remaining 4 are used for field shaping.

The first and the last cell of a chamber layer have a different setup. These cells have a trapezoidal shape. Printed circuit boards are mounted at the chamber walls as mesh planes. The momentum resolution in these regions is worse [32].

The MO–chamber is made of two times 21 drift cells with 16 sense wires. Nineteen cells with 16 wires build a MI–chamber. The MM–chambers contain two times 15 drift cells with 24 wires. The P–chambers show a single wire resolution of $\sigma_{wire} = 200 \mu$m. The resolution in a layer is given by $\sigma_{layer} = \frac{\sigma_{wire}}{\sqrt{N_{wire}}}$. Therefore the number of wires in the three layers takes the different contributions to the momentum resolution into account.

The z–chamber drift cells are of rectangular shape with a single wire in the centre. The cathodes are formed by aluminium I–beams of 6 cm height. The length of a cell is 9.23 cm. The resolution is 500μm [33].

A charged particle passing through the chamber ionises the gas molecules. The created electrons drift due to the electric field towards the sense wire. The drift velocity is nearly constant. As electric and Lorentz force act simultaneously on the charged particles, they travel on inclined tracks. The inclination angle is called Lorentz angle and has been measured to 18.55 ± 0.5^o [32]. Near the sense wires the electric field increases. The electrons gain enough energy to ionise itself. An avalanche is created. Due to this gas amplification a detectable pulse is obtained at the wire. When the drift velocity is known, the recorded drift time can be converted into a distance measurement.

The momentum measurement relies on the fact that a moving charged particle is deflected in a magnetic field due to the Lorentz force. If one uses a small angle approximation the distance S shown in figure 2.5 can be expressed as:

$$S = \frac{0.3Z}{8} \left(\frac{L}{[meter]} \right)^2 \frac{B}{[Tesla]} \frac{[GeV]}{P_t} \tag{2.1}$$

Here L is the distance between the outer points, B the magnetic field and P_t the transverse momentum.

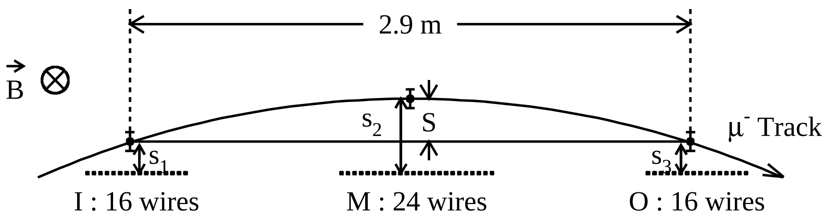

Figure 2.5: The definition of the sagitta S.

For the sagitta measurement a precise alignment of the three layers is essential. The relative position of the layers in one octant is assured by an optical alignment system. Unfortunately there exists no alignment between neighbouring octants and layers in different ferris wheels. Aligning these octants is unnecessary for particles coming from the vertex, but would be useful for cosmic ray tracks.

The distance between the centre of the outer MO and inner MI chamber amounts to 2.9 m. This lever arm results in a momentum resolution of 2.5 % at 45 GeV for tracks from the vertex that hit all three layers. The limiting contributions of energy loss and multiple scattering in detector parts has been taken into account. The resolution drops to 20 % for tracks measured only with two layers. The maximum detectable momentum (MDM) is 1.8 TeV. Here three layers hit are assumed. The MDM is defined as the momentum at which the measurement error is equal to the momentum itself.

2.3 T0 scintillator counter

The momentum resolution depends on the correct t0 time. The dependence on the shift in t0 time ΔT_0 can be expressed as [34]:

$$\frac{\Delta P}{P} \sim 6.4 \cdot 10^{-6} \cdot \frac{P}{[GeV]} \cdot \frac{\sqrt{\sigma_{intr}^2 + \kappa \cdot v_{drift}^2 \cdot \Delta T_0^2}}{[\mu\text{m}]} \tag{2.2}$$

The intrinsic resolution σ_{intr} of the sagitta S is determined by the single wire resolution, the chamber geometry and multiple scattering. A value of $\sigma_{intr} = 93\mu$m has been obtained. The parameter κ has been fitted to 0.50. The P-chamber drift velocity v_{drift} has been described in the previous section.

In normal LEP operation this t0 time is determined by the beam crossing. For cosmic muon events a new reference time is needed. This T0 signal is provided by scintillators placed on top of the magnets.

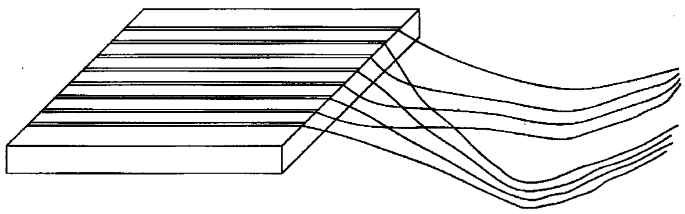

Figure 2.6: A picture of a scintillator tile. On top of the tile one can see eight 1.5 mm fibres glued into grooves. The fibres are divided into two groups read out by separate PMTs [35].

For phase I eight modules with 48 m^2 scintillator were planned to be placed above octant 2. The actual coverage is nine modules with 56 m^2. In the next step phase 1.5 this will be extended to 12 modules covering 72 m^2.

All three upper octants will be equipped in phase II. There are two 35 cm wide access ways between the modules. This divides the space above the magnet into four quadrants.

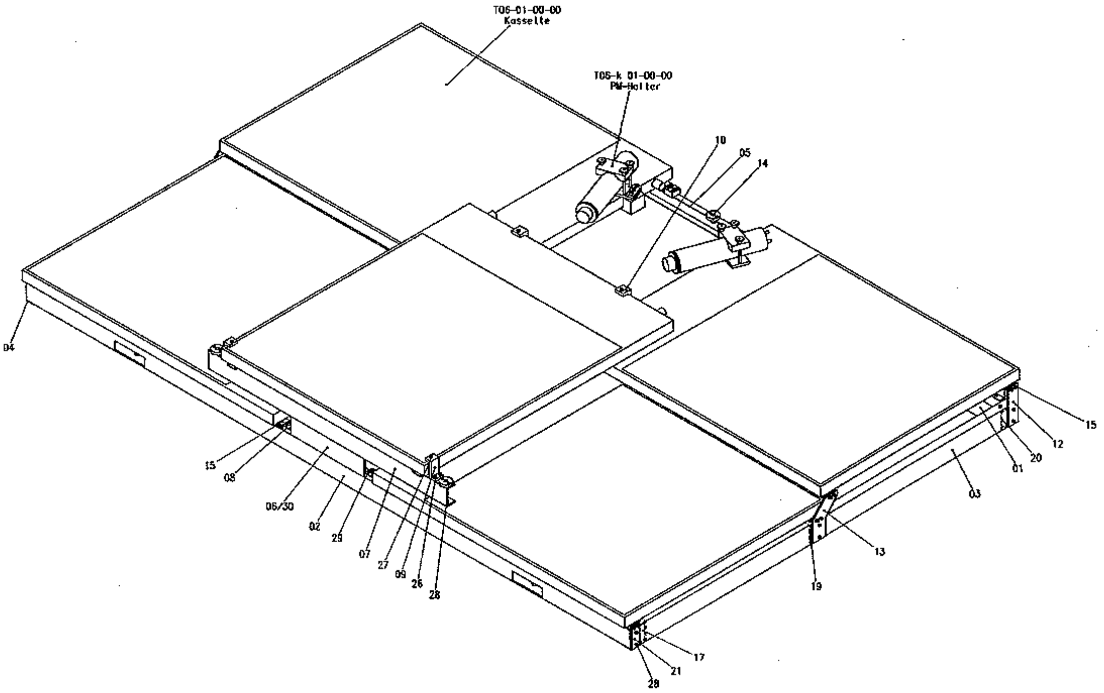

Figure 2.7: A picture of a t0 module.

A module is 3 m long and 2 m wide. A module contains six cassettes. Cassettes are mounted on the module frame at four different heights. This overlapping construction avoids holes in the structure. The cassette is formed by 4 times 4 tiles of plastic scintillator. Wavelength shifting fibres are glued into milled grooves on top of each tile. Tiles have dimensions 250 cm x 250 cm x 2 cm. A schematic view of a tile can be seen in figure 2.6. Two photomultipliers are used to readout the scintillators of a module. This redundancy is useful for timing improvement and noise suppresion. Requiring the coincidence of two PMTs reduces noise by more than one order of magnitude. The timing improvement is explained in more detail in section 5.1.8. The resulting time resolution is better than 1.5 ns.

2.4 Electronics

The L3+Cosmics data acquisition system has to be independent from normal L3 data taking. To satisfy this, the muon chamber signals are split after the preamplifier and read out separately.

The former muon personality cards (MPC) [36] are replaced by cosmic personality cards (CPC) [37]. A CPC card contains the same functionality as the MPC. In addition three 32–channel Time to Digital Converter (TDC) for 96 wires are installed [38]. These TDC's have a bin width of 25 ns/32 = 0.78 ns. The CPC card contains also a majority logic. This logic combines the wire signals. All arriving signals are stretched to 1.2 μs. This value corresponds to the maximal possible drift time: 50.5 mm/48 $\frac{\mu m}{ns} \sim 1\mu s$. If the number of recorded hits exceeds the programmed threshold a layer hit signal is generated. Each layer (MI, MM, MO) corresponds to a specific signal. To which layer a CPC card belongs has to be preset.

For scintillator signals a special CPC card is foreseen. On this special card no majority logic is present. Every eight inputs are connected by a logical OR instead. The resulting 12 signals are stretched and delayed to match the muon chamber signals. These outputs can be further combined to form a single scintillator hit signal.

The hit signals are fed into the Cosmics Trigger and Timing module (CTT) [39]. This unit determines the trigger class and accepts or rejects an event. A GPS receiver is installed as time reference. The Global Positioning System (GPS) is satellite based and delivers the precise world time. This makes correlations with other experiments very easy. The GPS signal is readout via the GPSTIM module.

Each CPC card is connected to a front end link (FElink) of a NIMROD (Nijmegen Monitored drift tube ReadOut Drive). The NIMRODs are used to read out the event. Each NIMROD contains 16 FElinks. For phase I four NIMROD's are installed. This will be extended to 16 NIMROD's for phase II.

2.5 Trigger and DAQ

There exist three trigger layers [40]:

- Level 1 Trigger (CTT card)
- Level 2 Trigger (VME master)
- Level 3 Trigger (HP Online Computer)

The level 1 trigger is a hardware trigger. The following trigger classes are implemented for phase I [39]:

Class	Description	Physics Interest
1	A triplet in octant2 AND NO scintillator hit	Yes
2	A doublet in octant2 OR octant6	Probably None
3	A triplet octant2 OR octant6	Yes
4	A doublet in octant2 AND octant6	May be

Doublets are defined as two muon chamber layers with hits. A triplet requires hits in all three muon chamber layers. These trigger classes can be separately enabled, prescaled or disabled. All classes can also be combined with the scintillator hit signal. This scheme is extended to all octants for phase II. Doublets in two neighbouring octants are also included.

Trigger level 2 is a software trigger. The online filter attempts an event reconstruction. This reconstruction has to be fast and is therefore rather crude. A cut on the reconstructed momentum can be performed [41].

Trigger level 3 is foreseen to check level 2 decisions.

Chapter 3

Simulation concept

A precision experiment requires a good simulation. The simulation is needed to understand the detector properties (e.g. acceptance) and to interpret experimental data. A main application is the comparison of experimental and theoretical distributions. The computer simulation also provides the possibility to test and improve the reconstruction (analysis) programs.

Quantum mechanical processes involve a certain “randomness”. Therefore a method based on random numbers is ideally suited to model events in high energy physics. Such methods are called “Monte-Carlo”-techniques.

The simulation procedure can be divided into four steps:

- particle generation at surface
- tracking through molasse
- detector simulation
- reconstruction

For the particle generation exist two approaches. If the primary flux is used as input, muons can be produced by a detailed simulation of the interactions in the atmosphere. Such an air shower simulation is CORSIKA. A faster generation is possible when the surface muon flux is parameterised and only muons are produced. Such a fast generator is L3CGEN.

Muons at surface level have to be transported through the molasse layer to obtain the distributions in the L3 hall. The fast approach is the program TRACK. Alternatively the detector simulation SIL3C can be used. The underground geometry is also implemented in SIL3C. This implementation is slightly more detailed, but slower. The detector simulation transforms the muons into an event. The last step is the reconstruction.

As L3+Cosmics is based on the L3 setup some of the experience gained in the years of successful operation can be transferred. The detector simulation and reconstruction are therefore based on existing L3 programs.

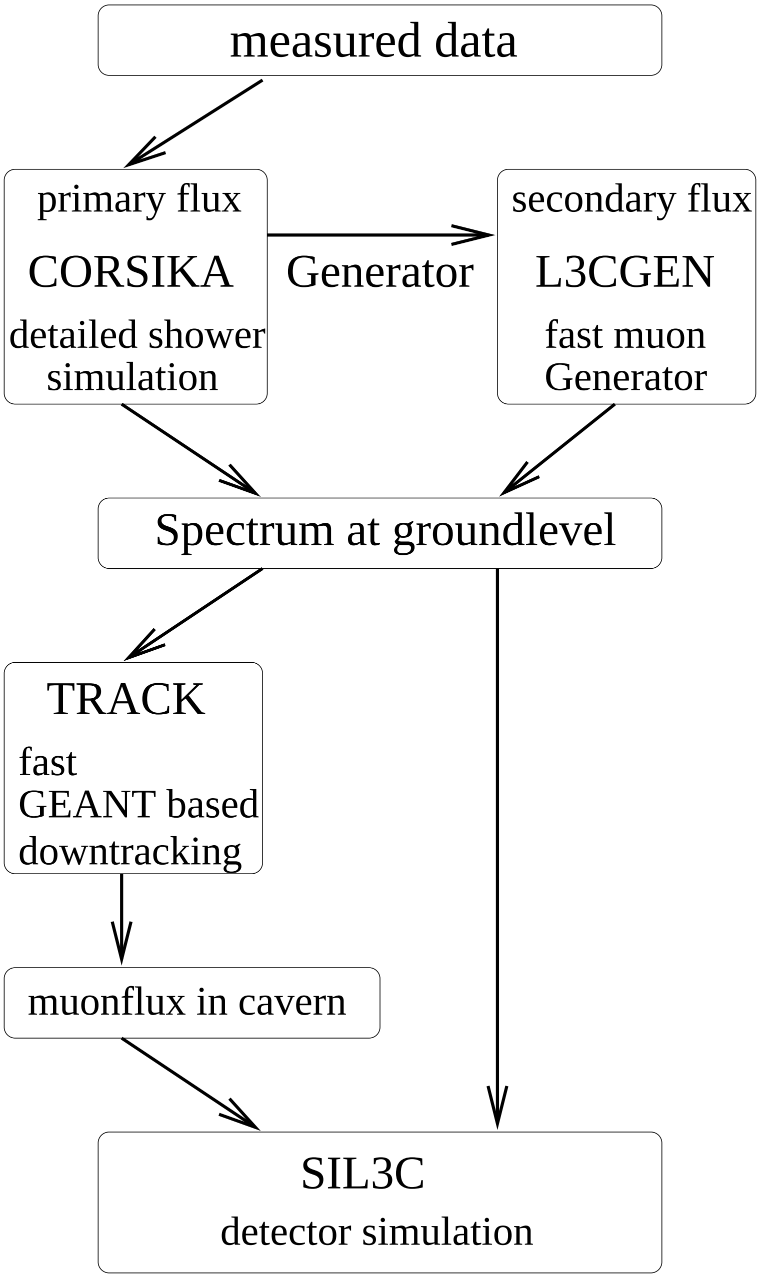

Figure 3.1: General simulation frame work for L3+Cosmics

Chapter 4

Generator

4.1 CORSIKA

A program widely used for simulation of extensive air showers is CORSIKA (COsmic Ray SImulations for KAscade)[42]. The program was developed for the KASCADE experiment[43]. It provides detailed information on shower content and development depending on the primary particle. The main drawback is the large amount of required computing time. The time to process one event strongly depends on primary type and energy.

primary energy	primary type	time per shower on HP735 excluding elm. cascades
500 TeV	iron	5 min
500 TeV	proton	3 min
5 TeV	proton	4 s

A variety of options allow to customise the simulation. These options are set using a data card with switches.

The coordinate system used has the z–axis up, x–axis to magnetic north and the y–axis to the west. The z–coordinate is measured with respect to sea level. Altitude of L3 surface level is 470m.

4.1.1 Shower simulation

Simulating the development of an air shower requires detailed treatment of particle transport, interaction and decay in a model atmosphere. The atmosphere used by CORSIKA is divided into 5 layers. The altitude dependence of the density in a layer is approximated by an exponential.

The first layer begins at 112.8 km height. The primary particle, of a type selected by the user, starts from this altitude. The energy is chosen at random from a power law distribution inside a given range. The slope of the distribution can be set by the user. The angular range can also be defined.

Secondary particles are tracked until they reach a user defined threshold. This threshold can be set separately for hadrons, muons, electrons and photons.

For tracking of the electromagnetic shower component the EGS-4 code is used. Due to the large number of particles to be tracked, the use of EGS reduces the program speed drastically. As an alternative an analytical treatment by the NKG formula is possible.

As the electromagnetic component is decoupled from the muon content, the simulation of this component has been switched off in simulations for L3+cosmics. It is only needed in photon induced showers.

The hadronic interaction can be treated by various models (VENUS, SIBYLL, QGSJET, DPMJET). A detailed description can be found in [42]. The VENUS model was chosen.

Particles are written to output if they cross an 'observation level'. Up to 10 different observation levels may be defined for a CORSIKA run.

4.1.2 Tiling

The lateral extension of a CORSIKA shower is rather large compared with the detector size. If no action is taken a large number of generated muons is lost. In order to use the invested computing time completely one CORSIKA event is transformed into several detector events by the tiling mechanism.

The surface coordinates of each particle are given by CORSIKA. The particle trajectories are extrapolated to a plane down in the depth of the L3 cavern parallel to the surface. This mechanism subdivides the shower area into squares of 50m length, so called tiles. The coordinates of particles in each square are then moved by the distance of the corresponding square to the middle. That means that every 50m times 50m area is treated as an independent detector. This is equivalent to smearing the shower axis with a fixed detector position [44].

4.2 L3CGEN

The program L3CGEN was coded in FORTRAN by T.Hebbeker [45]. This generator is based on parametrisations of energy and angular distributions of muons obtained via CORSIKA simulations. It is a very fast program. The speed is up to 1 million events per minute on a HP735. The generator is limited to single muon production.

The energy distribution is parametrised by a forth order polynomial. The energy dependent angular distribution is approximated by:

$$\frac{dN}{d\cos\theta} \sim 1 + a(E)(1 - |\cos\theta|) \tag{4.1}$$

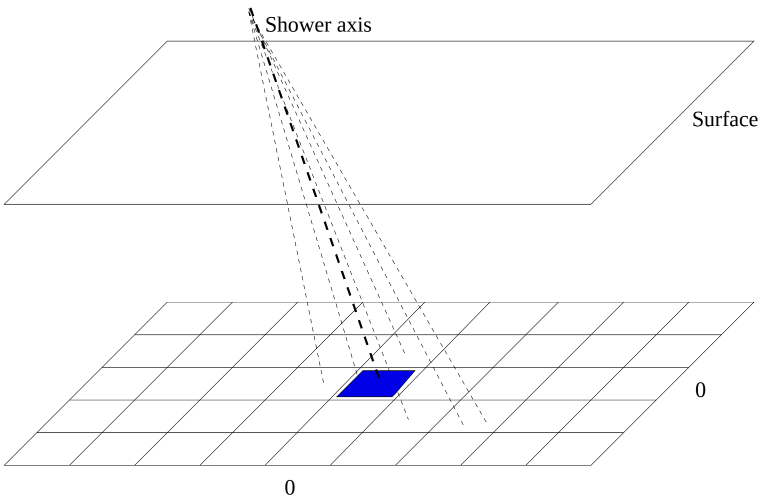

Figure 4.1: Only a few muons of a shower hit the detector situated at the origin.

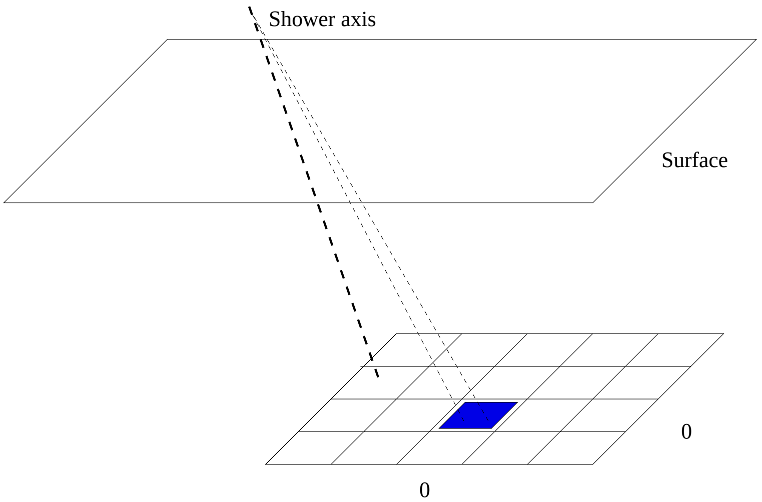

Figure 4.2: One of the subevents. The coordinate system has been moved.

Muons are generated with a fixed charge ratio of 1.3. The generator calculates the time interval corresponding to the number of generated events. This interval is obtained by counting events in the energy range 99.5 –100.5 GeV and comparing with the known vertical flux at 100 GeV $\Phi(E = 100GeV) = 2.8 \cdot 10^{-3} m^{-2} GeV^{-1} sr^{-1} s^{-1}$.

The generator allows a preselection. The widest option rejects muons outside a circle of 40 m radius around the detector underground. A simulation shows that no muons that hit L3 are lost. Tighter selections allow only muons that fall in an area compatible with the extensions of L3.

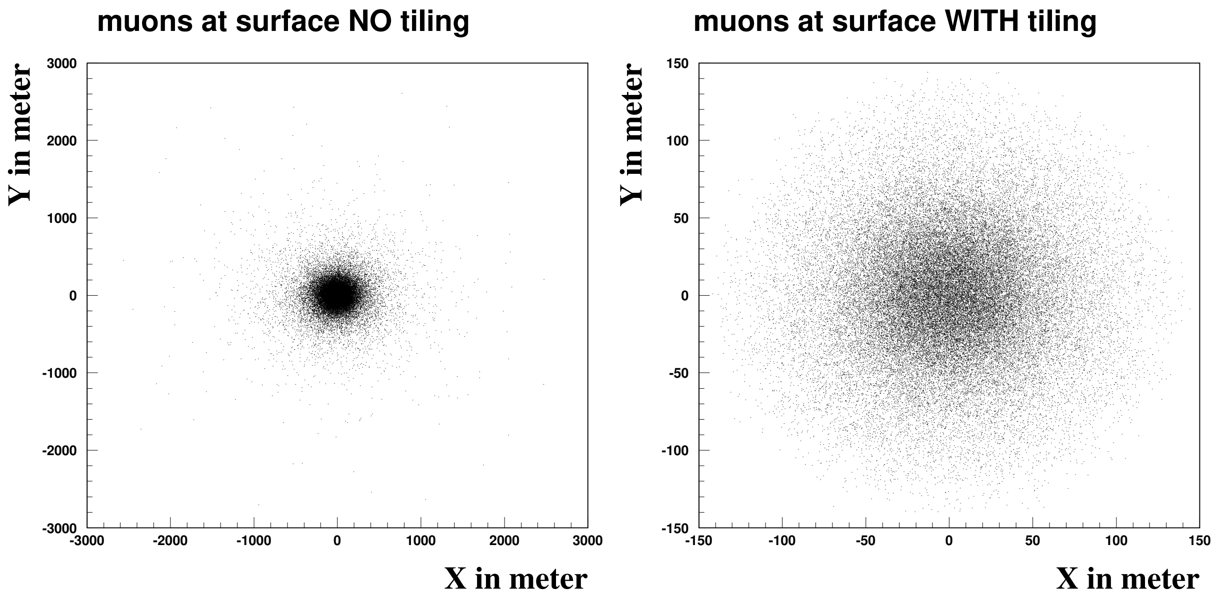

Figure 4.3: The spread of muons at surface: Left: without tiling a large area is covered. Right: the tiling mechanism reduces the spread.

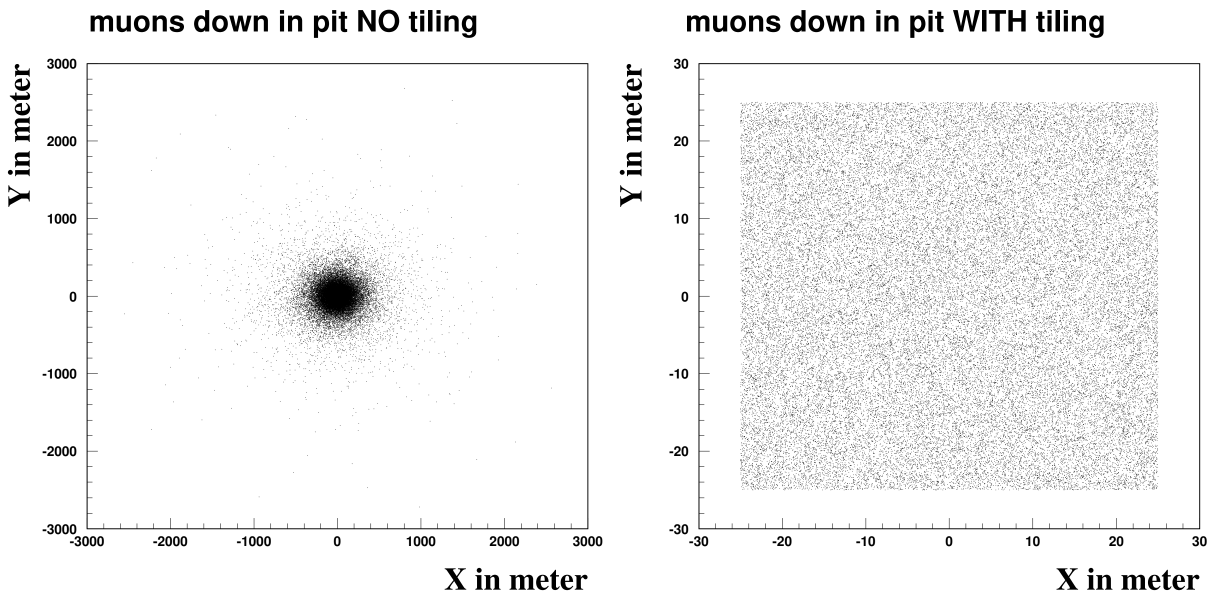

Figure 4.4: The space distribution of muons down in the L3 pit: Left: without tiling the muons are widely spread; only a small fraction lies inside the detector area. Right: with tiling applied muons hit all in a square of 50 m side length.

Muons are generated at the surface above L3. The particles have to be tracked down to the L3 pit. The speed makes this generator first choice for all studies that do not require information on shower processes. Investigations of systematical aspects of the experiment can be carried out with good accuracy using L3CGEN.

Chapter 5

Simulation of the L3+Cosmics setup

5.1 SIL3C

The L3+Cosmics detector simulation SIL3C is part of the cosmic analysis code COL3. The program has been adapted from L3 simulation code SIL3 version 211. The simulation is based on GEANT 3.53. It includes the t0 scintillator, the L3 detector and the surrounding molasse.

5.1.1 Description of detector volumes

The GEANT volume description of the setup is used in SIL3C, the reconstruction REL and the scan program. The top level volume MOTH is a sphere. Positioned inside mother are the surface layer SURF, the molasse layer with shafts MOMO and the L3 detector volume LEP3 . The tree of descendants from MOTH can be seen in figure 5.3. The LEP3 volume is formed by an octagon. The volume is subdivided into the following major regions:

- AREG (Additional setup)
- MREG (Muon chamber REGion)
- FREG (Forward REGion)
- HREG (Hadron calorimeter REGion)
- EREG (Electromagnetic calorimeter REGion)
- TREG (central Tracking chamber REGion)
- BVAC (Beam VACuum)

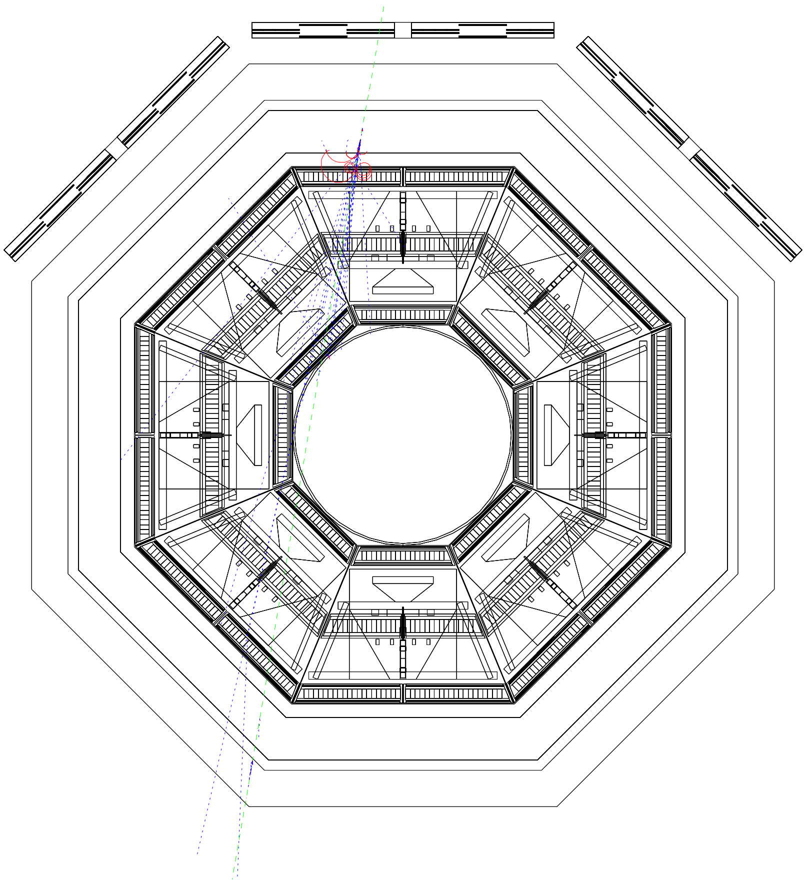

Figure 5.1: An event simulated with SIL3C. Shown in green is a 200 GeV muon track. Radiated photons are in blue, produced electrons and positrons drawn in red. The phase II setup with all three upper octants equipped with scintillator has been modelled.

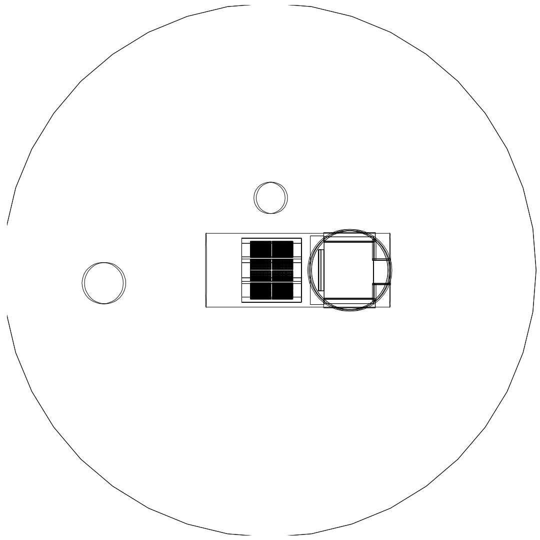

Figure 5.2: The main setup for SIL3C. Seen can be three shafts. Inside the main access shaft blocks of concrete are positioned. In the center the L3+Cosmics detector with a scintillator layer is visible inside the main hall. Two smaller shafts are positioned in the vicinity of the hall.

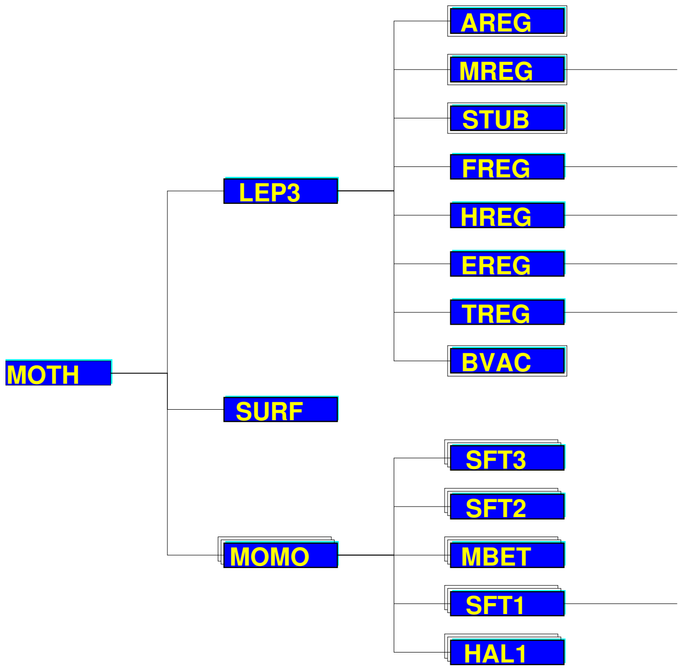

Figure 5.3: Tree of volumes descending from the mother volume.

5.1.2 Molasse volume

The volume MOMO is a sphere filled with molasse. The composition of the earth above L3 is well known. Several layers of different material are present, but the variations in density are very small. All layers have densities between $2.30 - 2.60\,\mathrm{gcm}^{-3}$. Layers with very low or high density are thin. As a good approximation an overall value of $2.40\,\mathrm{gcm}^{-3}$ can be used. This is also satisfied by the fact that additional material at the surface (e.g. buildings and cars) can not be taken into account easily.

The shafts and the L3 hall are implemented as air volumes. The main shaft of 23 m diameter houses a concrete structure. The two smaller shafts SFT2, SFT3 have radii of 5 m and 5.5 m respectively. The location of the shafts is shown in figure 5.2.

5.1.3 T0 counter

The top scintillator volume TSCN is positioned inside AREG 53.5 cm above the magnet. The complete structure of AREG can be seen in figure 5.4. The size of TSCN is variable according to the phase chosen. For phase II the volumes TSCL and TSCR identical to TSCN are positioned left and right. A realisation of the TSCN volume for phase II is shown in figure 5.5. TSCN is composed of four super modules SCSM each corresponding to a quadrant. Super modules on the left side are rotated by 180 degrees.

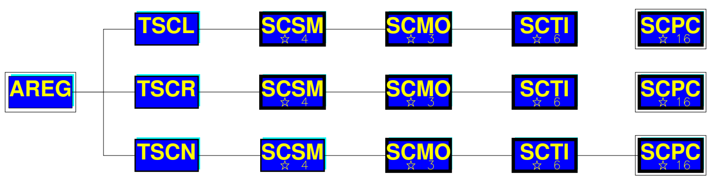

Figure 5.4: The volume tree in AREG.

The main building blocks are the scintillator modules SCMO. The geometry of such a module is drawn in figure 5.6. In SCMO six cassette volumes SCTI are placed at four different layers. Each cassette volume contains 4 times 4 tiles SCPC.

For phase 1 two modules are placed in a super module. For phase 1.5 and above a super module SCSM contains three SCMO modules.

Only scintillator tiles SCPC have plastic assigned as material. All other volumes are treated as air. They are used to simplify the treatment and correct assignment of hits to the real modules. The super modules numbering scheme assigns odd numbers to quadrants at positive x coordinates. The two highest numbered super modules lie in the positive z-direction. Modules are counted from the TSCN middle outwards.

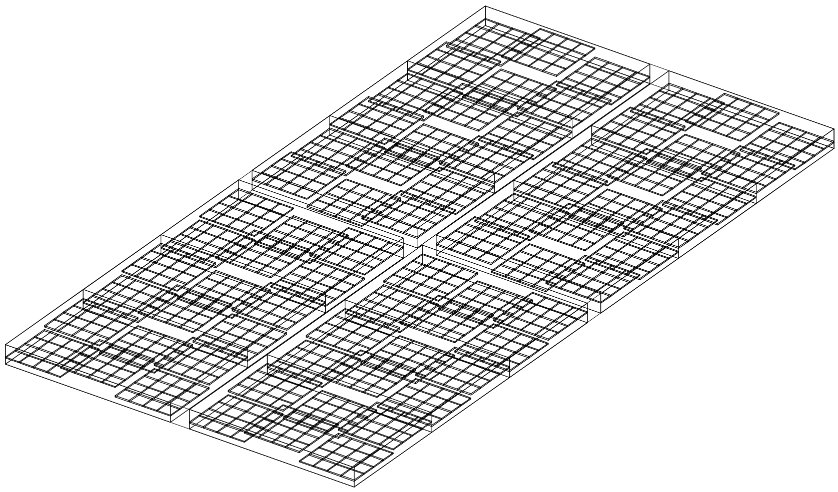

Figure 5.5: The top scintillator for phase 1.5 and 2. The two access ways can be seen easily. In phase 1.5 the top octant is equipped with 12 modules with together $72\mathrm{m}^2$ scintillator. The structure of such a module is shown in figure 5.6.

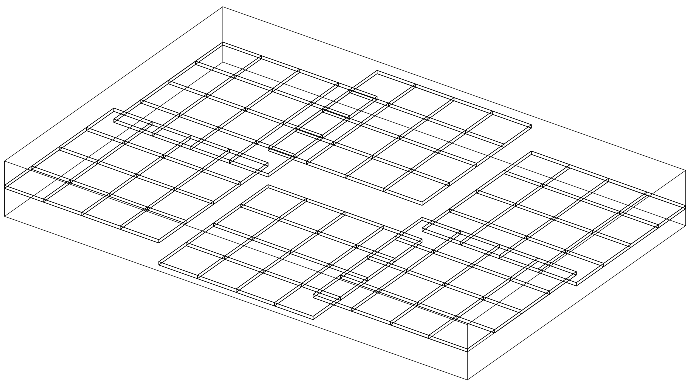

Figure 5.6: The model of a T0 module. The structure of the a real module is shown in figure 2.7.

5.1.4 Magnet

The magnet is described by the three volumes MGCO, MGDR and MGYK for coil, doors and yoke respectively. These volumes are positioned inside MREG. The material for MGYK and MGDR is iron. The coil volume MGCO is subdivided into 168 MGCD volumes. Into the middle of each air filled MGCD volume is an aluminium turn MGCA placed.

5.1.5 Muon chamber

The barrel muon chamber main volume called MBAR is also placed in MREG. This volume contains 16 octants MBFR. Each octant volume consists of the outer, middle and inner chamber volumes MBO, MBM, MBI, frame parts MAPL (A shaped plate) and MLGR (longeron).

The box MAPL is made of air and contains the top MBAT and bottom part MBAB of the A shaped plate. The volumes MBAT, MBAB and MLGR are aluminium.

The volumes MBO, MBM are trapezoids with angles 22.5 and 90 degrees (see figure 5.8). Two of these volumes form a chamber layer. The volume MBI is a trapezoid with two 22.5 degree angles and is a layer on its own. The octant volume MBFR is made of air, the chambers MBx and MLGR are aluminium (x=I,M,O).

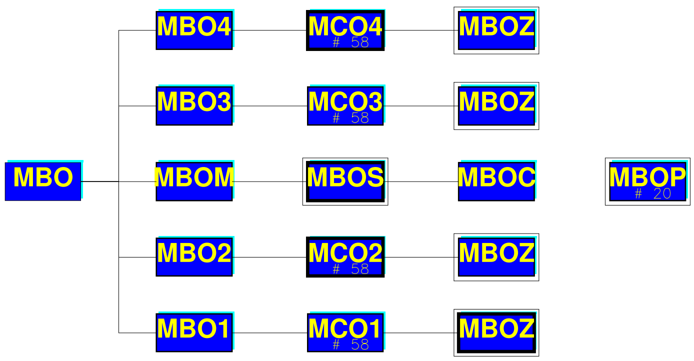

Figure 5.7: The volume tree of one side of an outer chamber. In a full layer two times 4*58 z cells and two times 20 + 1 P–cells are present. The 2 missing P–cells are the outer cells equipped with printed circuit boards

The chamber volumes are very similar. The four z–chamber layers are formed by MBOi and MBIi volumes for MBO and MBI respectively (i=1-4). The gas volume is contained in MCOi and MCIi. Z–chamber cells are approximated by MBOZ and MBIZ volumes. These volumes are the sensitive part of the z–

chamber setup. The middle chamber contains closing layers of special honeycomb aluminium MBMH instead of z–layers.

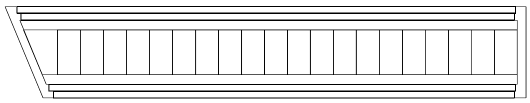

Figure 5.8: The MBO volume: The four z–layers can be seen. The chamber is divided into equal drift cells MBOP. The last trapezoidal shaped cell on the left is outside the MBOC volume.

P-chambers are modelled by a chain of MBxM, MBxS, MBXC and MBxP volumes (x=I,M,O). All these volumes are gas filled. The volume MBxS contains the sensitive region. P-chamber drift cells are approximated by MBxP. The volume MBxC contains all regular drift cells. Edge cells lie in the remaining space of the MBxS volume that is not filled by the box of MBxC. The simulation treats MBxP and MBxS as detector areas.

5.1.6 Simulation of detector response

The active detector parts include the muon chambers and the t0 scintillator. All other regions are treated as dead material in which the through going particles loose only energy.

Several effects have to be taken into account in order to model the response of the new t0 detector correctly. These include:

- fluorescent light production
- conversion into photoelectrons
- propagation effects
- influence of the digitisation and read out system

The simulation of the t0 detector response is described in detail in the next sections.

5.1.7 Hit combination

Energy depositions in active detector parts are recorded by GEANT. The depositions are given for each tracking step of a track. When a track enters a scintillator volume all depositions are added until the track stops or leaves the volume. The energies deposited by different tracks in the same sensitive volume have to be added as well. This is especially true for generated secondaries.

Figure 5.9 shows the energy depositions of different particles in the scintillator volume. Muons loose energy mainly by ionisation. The peak at 4 MeV corresponds to 2 cm scintillator. This is in good agreement with the assumption of a $\frac{\mathrm{dE}}{\mathrm{dx}} \sim 2$ MeV/cm for a minimal ionising particle. Muons can lose energy also by pair production and energy transfer to knock-on electrons, so called δ-electrons. Above a threshold of 1 MeV this process is treated as discontinuous energy loss and secondary particles are generated by GEANT. These losses are not recorded directly in the t0 detector. But the produced electrons deposit also energy in the scintillator. At low energies electrons loose their energy completely and stop in the material. All these energy depositions in a sensitive volume have to be added up. The smallest sensitive scintillator volume is SCPC. Finally the depositions in all SCPC volumes belonging to a module have to be added. The resulting distribution is shown in figure 5.10.

5.1.8 Pulse shape forming

The parameters delivered by GEANT have to be translated into a quantity which is comparable with the output of the electronics. The given parameters are the true time of passage for each track and the energy deposition in the active detector

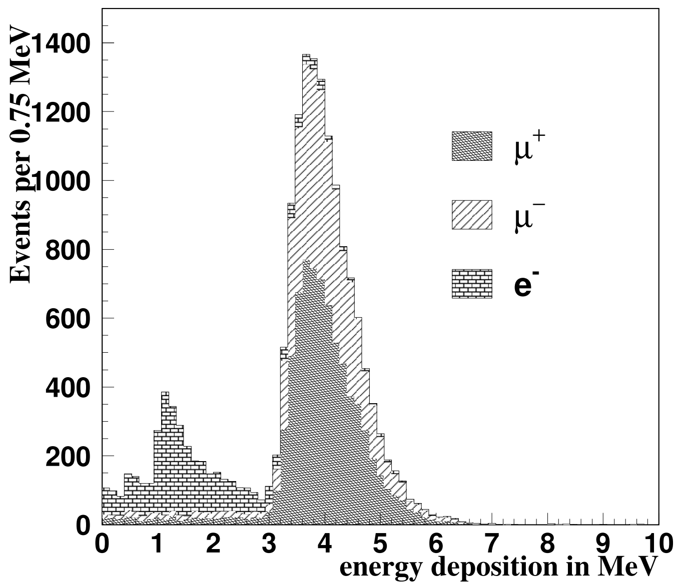

Figure 5.9: The energy deposition of particles in the scintillator.

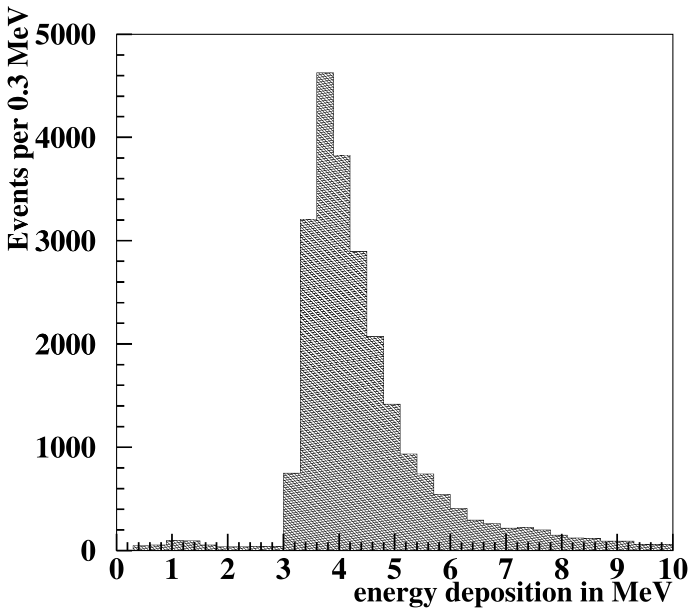

Figure 5.10: The total energy deposition of particles in the scintillator.

parts. The signal to be obtained is the corresponding TDC count (see section 2.4).

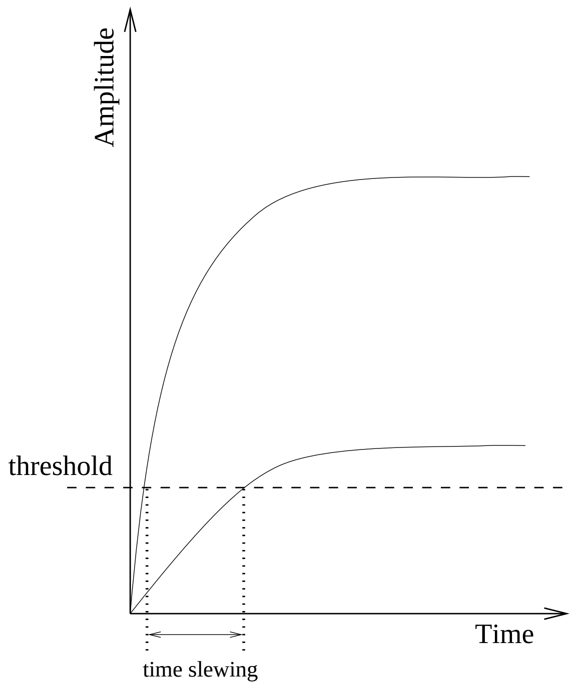

Figure 5.11: The effect of time slewing.

The first step scans all hits in a module. The earliest hit time is taken as signal start t_{sig}. Due to the effect of time slewing the time recorded by the electronics depends on the amplitude of the signal.

This effect can be understood with the help of figure 5.11. The discriminator of the electronics recognises a signal when it exceeds a certain threshold. All pulses raise with time and reach their maximal amplitude after a certain time. Pulses with a higher amplitude cross the threshold earlier than pulses with low amplitudes.

Measurements done at IfH Zeuthen are used for [46]. This effect has been parametrised as :

$$t_{tslw} = \left(0.44 + \frac{0.94}{a} - 1.38\sqrt{a}\right) ns. \tag{5.1}$$

Hereby is a the amplitude normalised to the mean value. The offset is arbitrary and has been choosen such that the correction vanishes for a mean amplitude $t_{tslw}(a = 1) = 0$. The amplitude has to be computed from the energy deposit. Measurements done at IfH Zeuthen form the basis for this parametrisation [46].

The light output of the scintillator is directly proportional to the energy deposited. Attenuation effects have been neglected since the read out of a tile by many wavelength shifting fibres assures nearly equal light travel times.

The number of photo electrons produced at the PMT cathode can be written as:

$$N_{\gamma_{calc}} = \frac{< N_\gamma > (channel) \cdot E_{dep}}{E_{mean}} \tag{5.2}$$

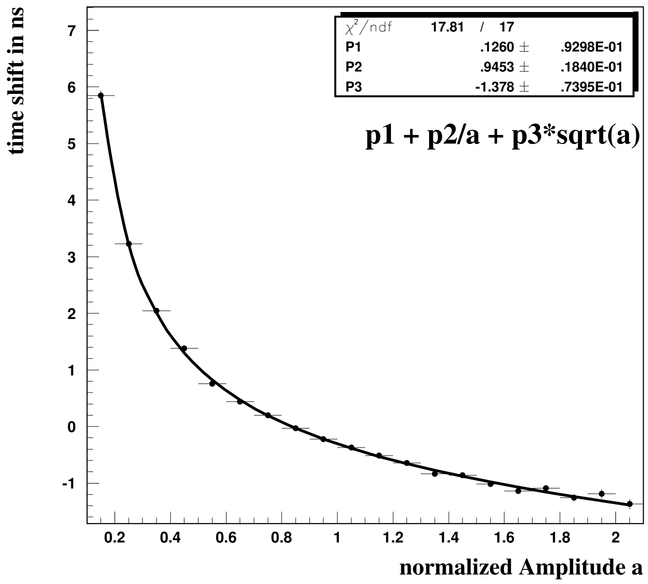

Figure 5.12: The parametrisation of the time slewing effect compared with data.

The average number of photo electrons has been measured to 7. This number depends on the used PMT. It is foreseen as separate parameter for each PMT channel. The mean energy deposit of $E_{mean} = 4.1\,\text{MeV}$ has been obtain from simulation. The number of photo electrons is Poisson distributed. The value N_γ used in further calculations is taken at random from a Poisson distribution with mean $N_{\gamma_{calc}}$.

The normalised amplitude a is given by:

$$a = \frac{A}{< A >} = \frac{N_\gamma}{< N_\gamma > (channel)}. \tag{5.3}$$

The time slewing correction is calculated combining equations 5.1 and 5.3.

Before the conversion into TDC counts a channel dependent Gaussian smearing t_{smear} and offset t_{offset} is added. The offset takes different cable lengths and propagation times in the electronics into account. The correction calculations are repeated for the second PMT. The time for each PMT 1,2 is given by:

$$t_{1,2} = t_{sig} + t_{offset}(channel) + t_{smear1,2}(channel) + t_{tslw1,2} \tag{5.4}$$

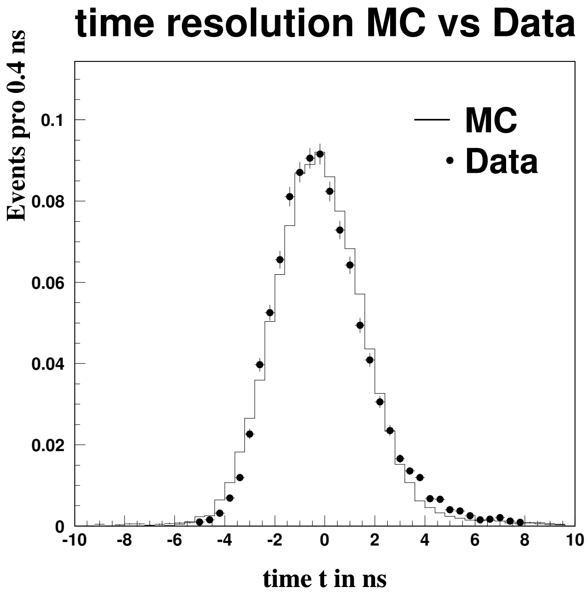

Figure 5.13: The time resolution Monte Carlo compared with data. Shown is the time distribution as measured by one PMT. The data sample was provided by the IfH Zeuthen.

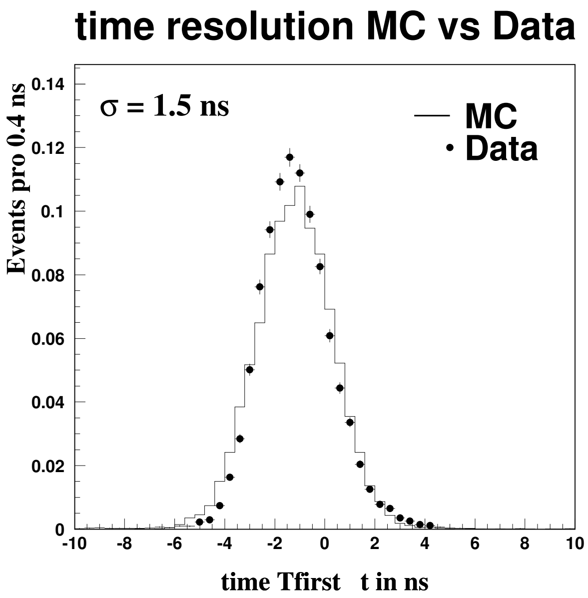

Figure 5.14: The time resolution of first arriving signal TFirst: Monte Carlo compared with data. Shown is the distribution min(T1,T2) of two PMTs.

This is converted into TDC counts via

$$TDC = t \cdot TDCSLOPE(channel) + TDCOFFSET(channel) \tag{5.5}$$

The size of a TDC bin is 25 ns/32 = 0.78 ns. The offset is assumed to be zero.

The constants have to be tuned for each PMT channel as soon as measurements for each module are available. In figure 5.13 a good agreement between data and Monte Carlo time distribution can be seen.

The time distributions that contain only the first of the two PMTs agree also rather well. The time Tfirst = min(T1,T2) is used for the t0 counters. The simulation can confirm the improvement in time resolution. None Gaussian tails are well suppressed with this technique.

5.2 TRACK

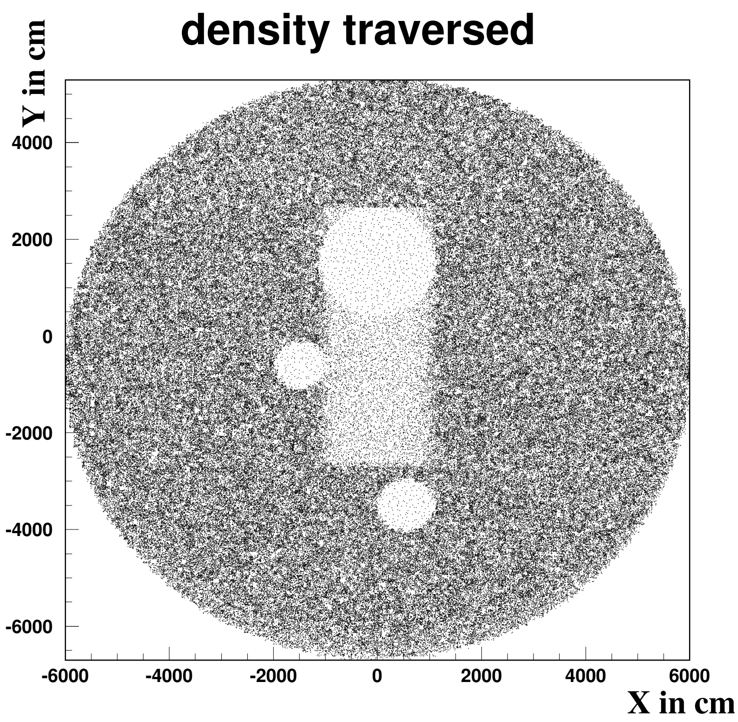

Figure 5.15: A muon x–ray of the setup underground. Shown is the density traversed by perpendicular incident muons of 200 GeV.

For propagating muons from the surface down to the L3-Detector the program `TRACK` is used. This program is based on GEANT [47]. Downtracking with `TRACK` is faster than with SIL3C. The reason is less overhead due to a shorter volume list. In addition GEANT 3.21 used for TRACK provides a better optimisation.

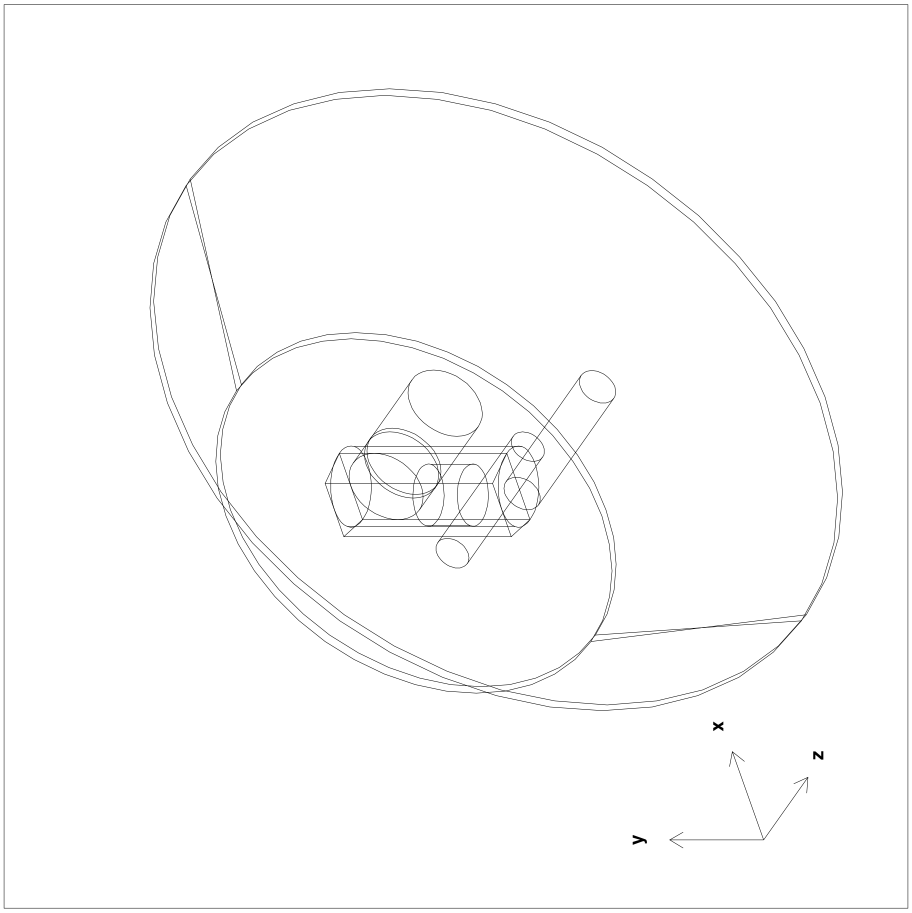

Figure 5.16: setup underground: Inside a cone of molasse three access shafts, the main hall and the LEP3 volume can be seen

The complete underground setup with all shafts is modelled. Surrounding molasse is approximated as a cone with a lower radius of 60 m and an opening angle of 60^o (see figure 5.2). The molasse composition is the same as in SIL3C. An average molasse density of $2.40\,\mathrm{gcm}^{-3}$ is assumed.

Three shafts are present. The main shaft of 23 m diameter and two smaller shafts of 5 m and 5.5 m radius respectively. The location of these shafts can be seen in picture 5.15.

The 1.39% slope of the L3 experiment are taken into account. The program is able to read different data formats. It can read CORSIKA data and L3CGEN formats. These data formats are recognised using the file extension.

In a CORSIKA file all showers point to the origin. To allow a realistic simulation the primary vertex can be smeared by TRACK in a circle of 120 m diameter.

The input routine of `TRACK` allows also an event selection. Only particles that hit inside a circle of 40 m radius around the L3 volume underground are tracked when this mechanism is selected. As this rejects a large number of events it is possible to repeat the smearing until a track is not rejected. The division of the hit area into tiles and the treatment of these tiles as independent detector areas is equivalent to the smearing of primary vertices. This tiling method is more efficient (see section 4.1.2).

The output contains the particle coordinates in the selected stop volume. Two possibilities can be enabled: The LEP3 volume, a cylinder of 9.5 m radius and 14.2 length and TSCN a box of 12.35 m x 6.35 m x 0.33 m. The particles are stopped at the borders of the volume. Output coordinates are L3 coordinates. The format used is described in chapter B.1. If histogram output is selected the amount of matter traversed by the muon can be plotted. Figure 5.15 shows as example a muon x–ray picture of the setup. Shown is the density traversed by perpendicular incident muons of 200 GeV.

Chapter 6

Results

6.1 Angular resolution

A good angular resolution is needed to observe the moon shadow and search for point sources. The angular resolution of the experiment is limited by multiple scattering in the molasse layer. In order to obtain a reliable estimate of achievable resolution muons have been generated using L3CGEN and tracked through the molasse with TRACK. The deflection at different energies and directions has been recorded. A Gaussian has then been fitted through the deflection angle distribution of each bin. An example is shown in figure 6.1.

energy GeV	traversed density g/cm^2	real density gaussian width 10^{-4}	$X = X_0 \cdot \cos\theta$ gaussian width 10^{-4}
100-170	7200-7700	26.80 ± 0.33	25.17 ± 0.35
100-170	7700-8200	27.42 ± 0.35	25.87 ± 0.53
100-170	9200-9700	31.50 ± 0.44	32.90 ± 0.80
100-170	9700-10200	33.28 ± 0.48	34.13 ± 0.85
170-240	7200-7700	16.47 ± 0.40	14.71 ± 0.43
170-240	7700-8200	16.08 ± 0.42	15.13 ± 0.69
170-240	9200-9700	19.22 ± 0.51	17.80 ± 0.79
170-240	9700-10200	19.98 ± 0.54	19.66 ± 1.18
230-300	7200-7700	11.84 ± 0.51	11.35 ± 0.51
230-300	7700-8200	12.58 ± 0.50	11.39 ± 0.70
230-300	9200-9700	13.77 ± 0.59	13.87 ± 1.03
230-300	9700-10200	15.18 ± 0.62	13.71 ± 1.40

The angle used is the scattering angle projected onto a plane. This angle can be calculated from the momentum vectors at the surface and in the pit via:

$$V_{proj_{x,y}} \cdot \frac{\vec{P}^{in} \cdot \vec{P}^{out}}{|P|^2} = \frac{P^{in}_{x,y} \cdot P^{out}_{x,y} + P^{in}_{z} \cdot P^{out}_{z}}{|P|^2} = \cos\theta_{plane_{x,y}} \tag{6.1}$$

The angle θ_{plane} follows a Gaussian distribution.

The deflection angle in space

$$\frac{\vec{P}^{in} \cdot \vec{P}^{out}}{|P|^2} = \cos\theta_{space} \tag{6.2}$$

is connected with the scattering angles in a plane via:

$$\theta_{space} = \sqrt{\theta^2_{plane_x} + \theta^2_{plane_y}}. \tag{6.3}$$

The angle θ_{space} is distributed as

$$\frac{dN}{d\theta_{space}} \sim \theta_{space} \cdot e^{-\frac{\theta^2_{space}}{2\sigma_s{}^2}}. \tag{6.4}$$

Where σ_s is the same as for θ_{plane}.

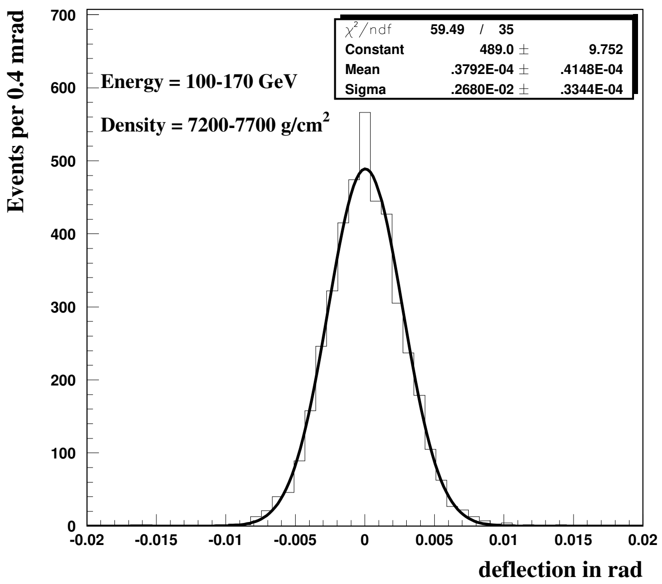

Figure 6.1: Distribution of the scattering angle θ_{plane}. Shown is the distribution for the lowest energy and traversed density bin.

The width σ_s increases with more traversed material and decreases with higher energy:

$$\sigma_s = c \cdot \frac{1}{E}\sqrt{X} \tag{6.5}$$

Here X is the traversed density in gcm^{-2}. Assuming this dependence the constant c has been fitted using MINUIT [48]. Due to binning an average has to be used.

$$\int\int \sigma_s(E,X)dEdX = <\sigma_s> \int\int dEdX \tag{6.6}$$

$$<\sigma_s> = \frac{\int_{X_1}^{X_2}\int_{E_1}^{E_2} c\cdot\frac{1}{E}\sqrt{X}dEdX}{\int_{X_1}^{X_2}\int_{E_1}^{E_2} dEdX} = \frac{c(X_2^{\frac{3}{2}} - X_1^{\frac{3}{2}})(\ln E_2 - \ln E_1)}{(X_2 - X_1)(E_2 - E_1)} \tag{6.7}$$

The fit results in the following parametrisation of $<\sigma_s>$:

$$<\sigma_s> = (3.37 \pm 0.02)\mathrm{mrad}\cdot\frac{100\mathrm{GeV}}{\mathrm{E}}\sqrt{\frac{1}{\cos\theta}} \tag{6.8}$$

It has been assumed here that the density X is given by $X = 6900\,\mathrm{gcm}^{-2}\cdot\cos\theta$. The value $6900\,\mathrm{gcm}^{-2}$ corresponds to a depth of 28 m in a material of $2.40\,\mathrm{gcm}^{-3}$. This are the parameters of the molasse layer above L3.

The dependence of X on $\cos\theta$ is slightly more complicated due to the shafts. The validity of the used approximation has been tested, repeating the fit with density bins substituted by $X = 6900\,\mathrm{gcm}^{-2}\cdot\cos\theta$. The resulting deflection is slightly lower, but agrees with equation 6.8. The lower deflection can be explained by the lower amount of traversed material in shaft regions.

The resulting angular resolution of the L3+Cosmics apparatus is still excellent compared with other experiments. For example MACRO has a resolution of 0.9 degrees [22]. The prospects to search for point sources or the shadow of the moon are therefore good. For charged particles the deflection in the earth's magnetic field is by a factor of five larger [49]. The angular resolution of the detector has no influence on measurements of the differential muon spectrum, for which a binning of 5 degrees has been proposed [18].

6.2 Energy loss

Before cosmic muons reach the L3+Cosmics detector they have to pass through a certain amount of matter. They loose energy during this travel.

The angular dependence of the energy loss is determined by the overlying material. This can be clearly seen in figure 6.3. The reconstruction uses the same model of the molasse layer as the simulation. For the different average energy loss can therefore be corrected. But the fluctuations of the energy loss of muons in the molasse layer set limits on the achievable momentum resolution.

A sample of 4 million muons with a lower energy threshold of 2 GeV has been propagated through the underground setup with `TRACK`. The resulting distributions of the energy lost are shown in figure 6.2.

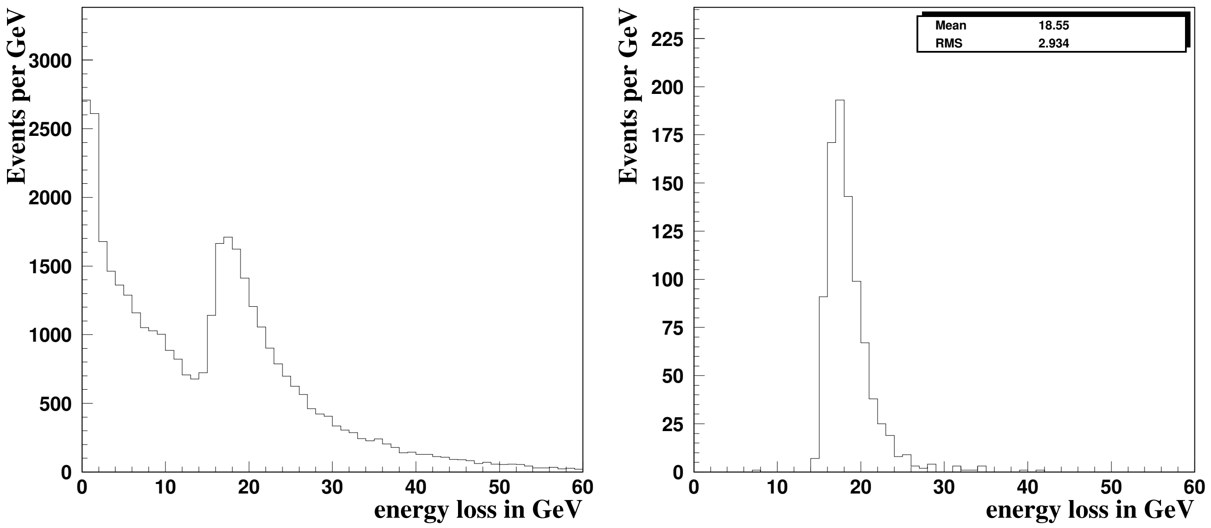

Figure 6.2: Left: Energy loss distribution of all particles arriving in the detector volume. Particles travelling through shafts loose less than 15 GeV. Right: Distribution of energy loss for particles arriving under $\cos\theta > 0.9$ from the direction opposite to the main shaft $\phi \sim 0$. These particles travel through approximately the same amount of material. The width of the distribution is a measure of the energy loss fluctuations.

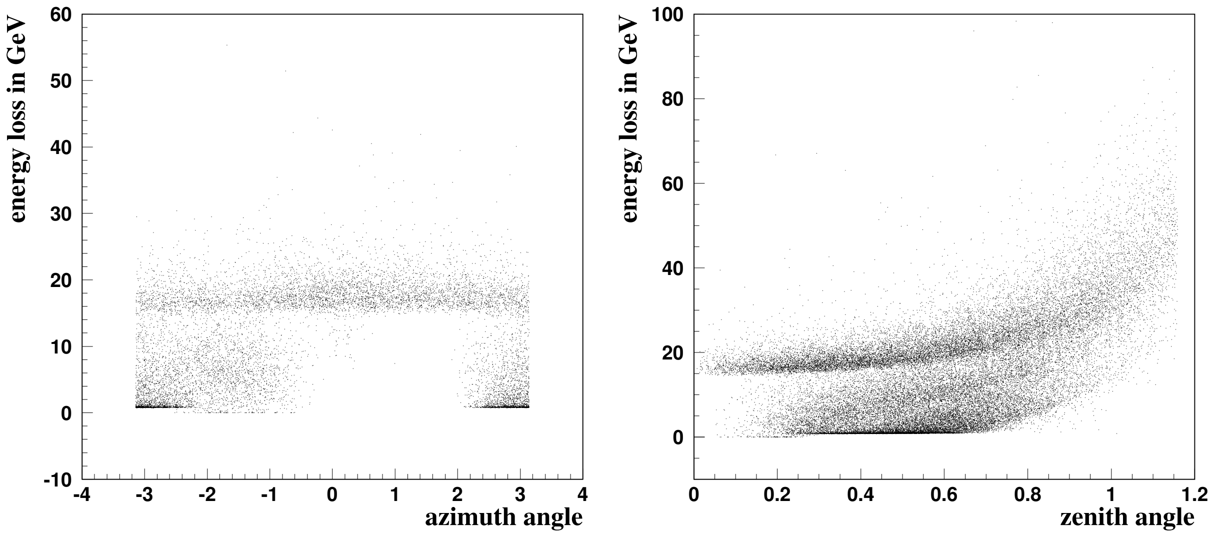

Figure 6.3: Left: The azimuthal distribution of lost energy. Particles travelling through the main shaft at $\phi = |\pi|$ loose only a small amount of energy in the concrete layer present. Some of the particles travel through the side shaft with no energy loss. Right: Zenith angle distribution of energy loss. The loss increases with $\frac{1}{\cos\theta}$ proportional to the overlying molasse layer.

Muons that come from close to above have been selected to get an estimate of the fluctuations.

Muons arriving from shaft directions have been excluded. The width of the resulting distribution corresponds to the systematic error that has to be added to the measured momentum. This error amounts to 3 GeV nearly independent of energy. This uncertainty becomes important below 75 GeV. At this energy the uncertainty due to energy loss fluctuations is of the same order as the intrinsic momentum resolution.

6.3 Acceptance

In order to derive the correct flux a detailed understanding of the detector acceptance is essential. Large muon samples with a realistic spectrum have been generated with L3CGEN. The samples contain 4 million muons after a preselection done by L3CGEN. Only muons that fall in a circle of 40 m radius around the underground detector area are taken. The resulting rejection factor is 10.56.

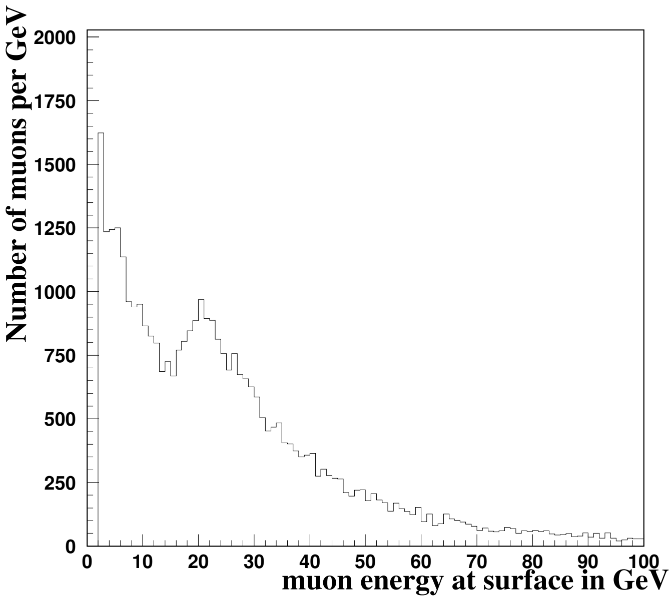

Figure 6.4: Energy distribution of accepted muons at surface. Muons below 15 GeV are shielded by the molasse layer.

Two samples with lower energy thresholds of 2 GeV and 20 GeV have been produced. The threshold of 2 GeV has been chosen because it is the lowest muon momentum which can be generated by L3CGEN with reasonable accuracy. The 20 GeV sample was used to improve the statistical error. The molasse layer above L3+Cosmics forms an absorber for muons with energy less than 15 GeV. As the energy spectrum is very step most muons are produced at the lower threshold. For these reasons only a small fraction of muons from the 2 GeV sample reach the detector area.

hit pattern	eff. Area
PHASE I	
20 GeV cut-off	
3 hits in oct3 & oct7 + t0	2.67 ± 0.08 m^2
3 hits in oct3 & oct7 (same ferris wheel) + t0	1.95 ± 0.07 m^2
3 hits in oct3 or oct7 + t0	16.3 ± 0.2 m^2
3 hits in oct3 or oct7 (same ferris wheel) + t0	15.1 ± 0.2 m^2
2 GeV cut-off	
3 hits in oct3 or oct7 + t0	1.82 ± 0.06 m^2
PHASE II	
20 GeV cut-off	
3 hits in one upper & one lower oct + t0	12.14 ± 0.35 m^2
3 hits in one upper & one lower oct (same ferris wheel) + t0	11.1 ± 0.35 m^2
3 hits in any oct + t0	42.1 ± 0.7 m^2
3 hits in any oct (same ferris wheel) + t0	39.4 ± 0.6 m^2
3 hits in any oct + topt0	21.65 ± 0.47 m^2
3 hits in any oct (same ferris wheel) + topt0	20.01 ± 0.45 m^2
2 GeV cut-off	
3 hits in any oct + t0	4.1 ± 0.1 m^2

Table 6.1: The calculated effective areas for various cases. Errors quoted are statistical only.

Low energy muons are important in areas with shafts where no absorber is present. This can be seen in the angular distribution of low energy muons in figure 6.6. The top of the L3 hall is located at 28.75 m depth. The main access shaft has 23 m diameter. This corresponds to an angle of 0.64 rad. The distribution shows a clear maximum at this angle.

The effect of the two other shafts is visible only in the azimuth angle distribution. These effects vanish for high energy muons.

The surface energy of accepted muons shows a dip around 15 GeV (see figure 6.4). At lower energy only muons travelling through the shafts reach the L3 pit and the acceptance is reduced. This causes a shift in the spectrum.

energy in GeV	integral flux in $m^{-2}s^{-1}$ster−1	correction factor	total flux in $m^{-2}s^{-1}$
2	520	0.6	312
100	0.13	3.7	0.49
1000	$5.2 \cdot 10^{-4}$	5.6	$2.9 \cdot 10^{-3}$

Table 6.2: Muon flux taken from [50].

The acceptance is obtained in form of an effective area. The effective area is given by the surface area onto which muons are generated weighted with the ratio of accepted to generated muons. To avoid a bias the generation area has to be large. The used generator L3CGEN produces muons on a spherical surface area of $2\pi \cdot (130\text{m})^2 = 106185\text{m}^2$. A realistic spectrum has been used.

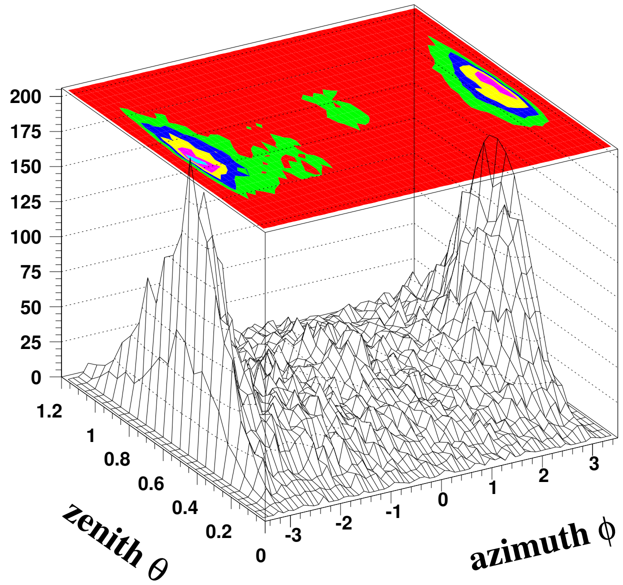

Figure 6.5: Angular distribution: Shown are the number of muons in zenith versus azimuth angle. The main shaft is located at $\phi = |\pi|$. The muon energy starts at 2 GeV

The effective area has some major advantages over geometric definitions. All physical effects, especially the absorption of low energetic muons, are taken into

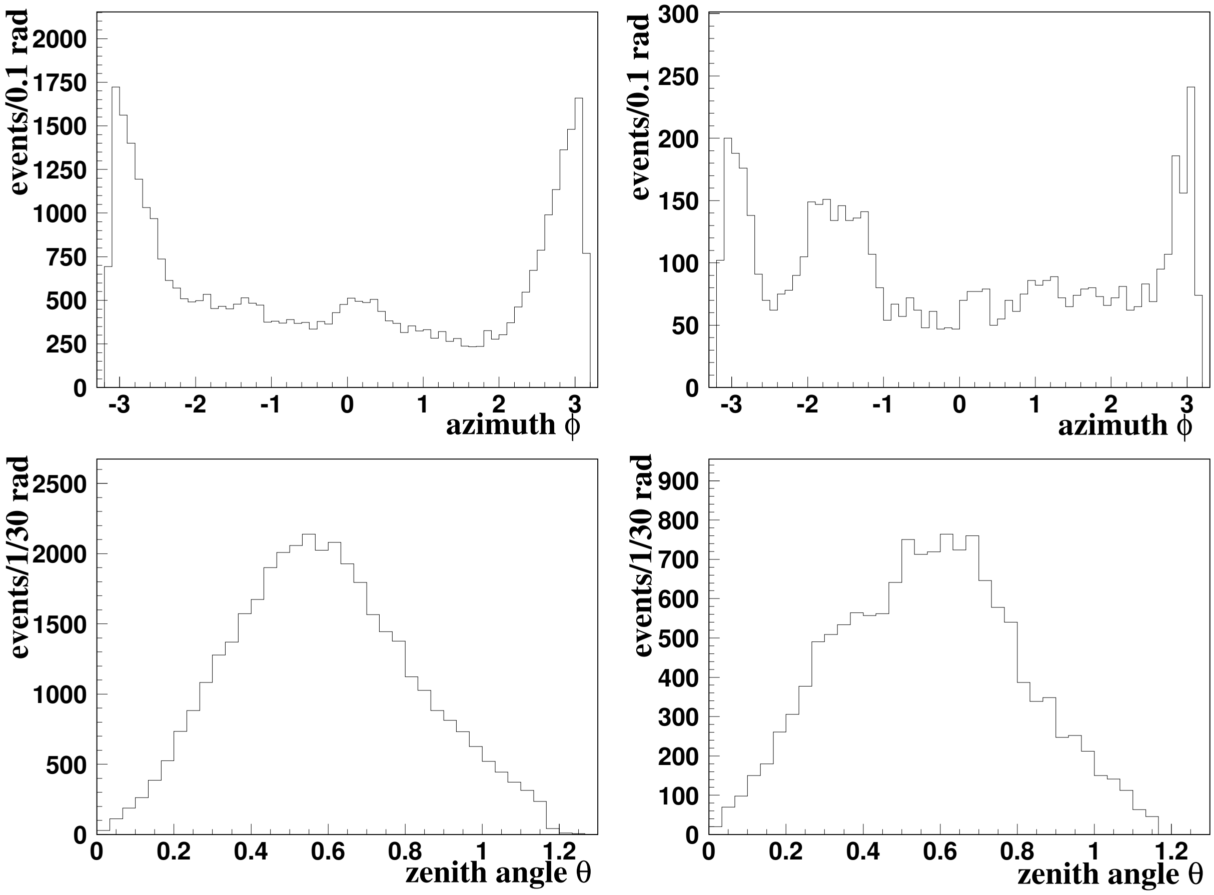

Figure 6.6: The angular distributions of the low energy muon sample reaching L3. The location of the three shafts can be seen. The left histograms show the distribution inside the L3 pit. The right picture shows the distribution of muons that hit Phase II scintillator and 3 muon chamber layers.

account. Rates can be obtained very easily by multiplying the effective area with the surface muon flux.

The integral flux given in [50] is here used. As the values given corresponds to the flux in the near vertical region A correction factor has been applied to take the angular variations of the flux into account. The correction factor was calculated using equation 4.1. The flux results in a rate of 8 Hz (0.05 Hz) for muons above 100 GeV (1000 GeV) in Phase I. For phase II the rate increases to 21 Hz (0.1 Hz) for muons above 100 GeV (1000 GeV). This means that in an effective running period of 1 yr = 86400 s 4000 events above 1 TeV are taken with phase I. This number more then doubles to 8400 for phase II. Therefore a statistical accuracy of at about 2 percent in total flux at this energy is possible. The angular distribution can also be measured with reasonable accuracy.

For phase I 72 m^2 scintillator is assumed. Phase II consists of 3 times 72 m^2 scintillator. Three hits in any octant mean that a track hits all three chambers.

6.4 Multi muon events

The study of multi muons is the most promising tool to obtain information on the primary composition.

An iron nucleus can be treated as the superposition of 56 nucleons with energy $\frac{E}{56}$. As the cross section for meson production rises only logarithmically with energy an incident proton produces less particles than an iron nucleus of the same energy:

$$\ln E < 56 \cdot \ln \frac{E}{56} \tag{6.9}$$

This effect allows to test different composition models.

But the particles are distributed over several hundred meters. The question is if the difference is still observable in a detector of limited size. The theoretical uncertainty in the simulated distribution plays also an important role.

For this investigation 1 million proton and 100000 iron showers have been generated. Muon energies above 100 GeV were required. This should reduce shaft effects. The energy range was set to 150 GeV-10^4 TeV for protons and 5 TeV-10^4 TeV for iron primaries. The reason for the difference in the energy range is a low energy cut of in CORSIKA around 80 GeV per nucleon. The different shower numbers are due to the fact that iron showers consume more computing time. For the simulation CORSIKA v5.20 with GEISHA and VENUS has been used.

The underlying hadronic interaction model has large influence on the observed muon multiplicity.

It is important to check the systematics. With CORSIKA a wide variety of models can be tested. A detailed analysis can be found in [51].

After the application of the tiling mechanism multiplicities up to ~ 100 survived in a grid of 50 m times 50 m. The multiplicity distribution is shown in figure 6.7.

Downtracking to the L3 pit with track preserved multiplicities up to 18. Protons produce maximal muon doublets in the detector. The corresponding distributions are shown in figure 6.8.

But multiplicity is strongly dependent on the energy of the incident primary. The number of high energy primaries is low and underlies large fluctuations. The statistics obtained corresponds only to a very short period of data taking (roughly 5h).

The observed ratio of single to multi muon events of 2 % is in good agreement with data obtained during the BGO calibration run [34]. In the year 1991 a dedicated cosmic run took place. It was used to calibrate the electromagnetic BGO calorimeter [52]. In this data a maximal multiplicity of 13 has been recorded so far. This lies in the predicted range.

The efficiency of multi muon reconstruction plays an important role. Unfortunately this could not be studied so far. As main problem remains Monte Carlo

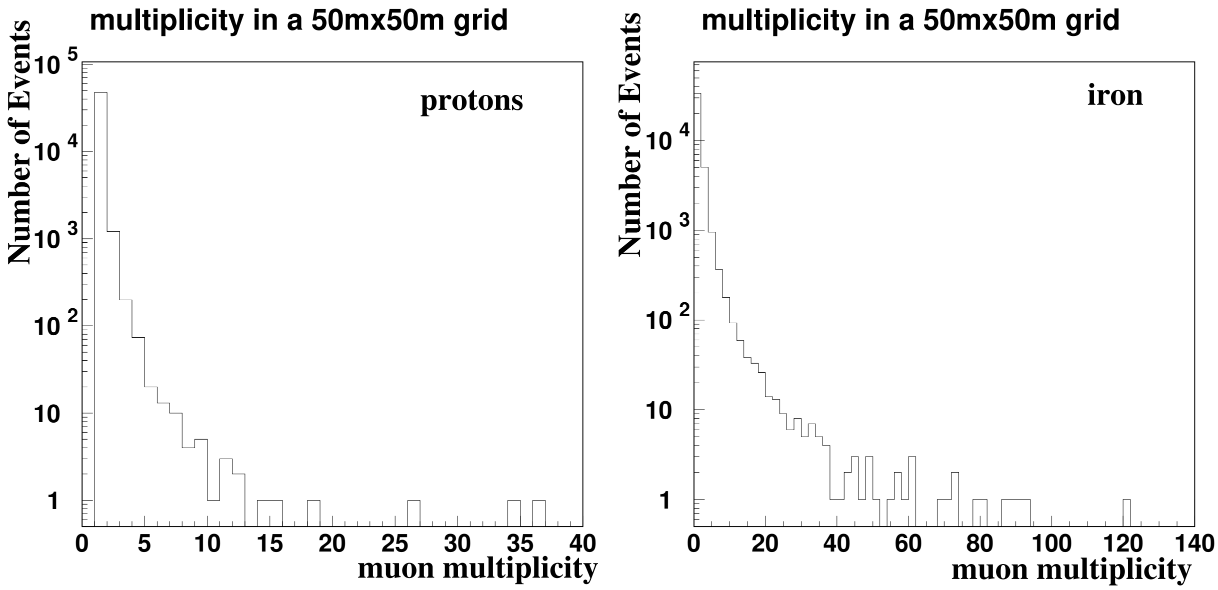

Figure 6.7: Muon multiplicity in a 50 m times 50 m grid for different primaries.

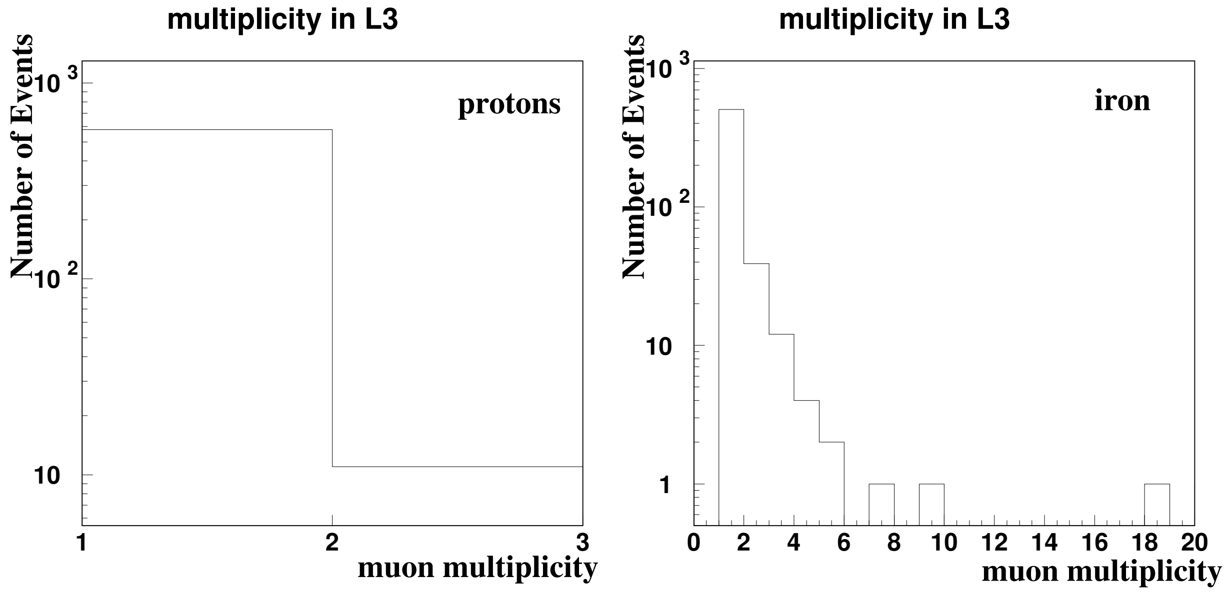

Figure 6.8: Muon multiplicity in the L3 detector volume.

statistics.

Looking into correlations with muon energy is another interesting possibility to study the primary composition. The analysis of muon families is a stronger tool, than multiplicity alone [53]. Further studies with better statistics are needed.

Chapter 7

Summary and Outlook

The experiment started operation in the middle of July. The hardware installation of the L3+Cosmics experiment is nearly finished. The first data have been taken with a simplified read out. One of the first reconstructed events is shown in figure 7.1.

Phase I will be completely installed by the beginning of august.

The reconstruction and simulation programs are ready. Further improvements require the comparison with data.

A detailed description of the material in buildings above the L3 area could improve the reliability of acceptance and energy loss calculations. The fine tuning of constants describing the scintillator simulation on the basis of measurements could lead to a better agreement between data and Monte Carlo.

It has been shown, that precise measurements of the muon flux are possible with the L3+Cosmics experiment. Most previous estimates of momentum and angular resolution agree with this newer investigation. More studies are needed on the subject of multi muons. Higher Monte Carlo statistics and a detailed analysis of the model dependence are necessary before conclusions on the primary flux can be drawn.

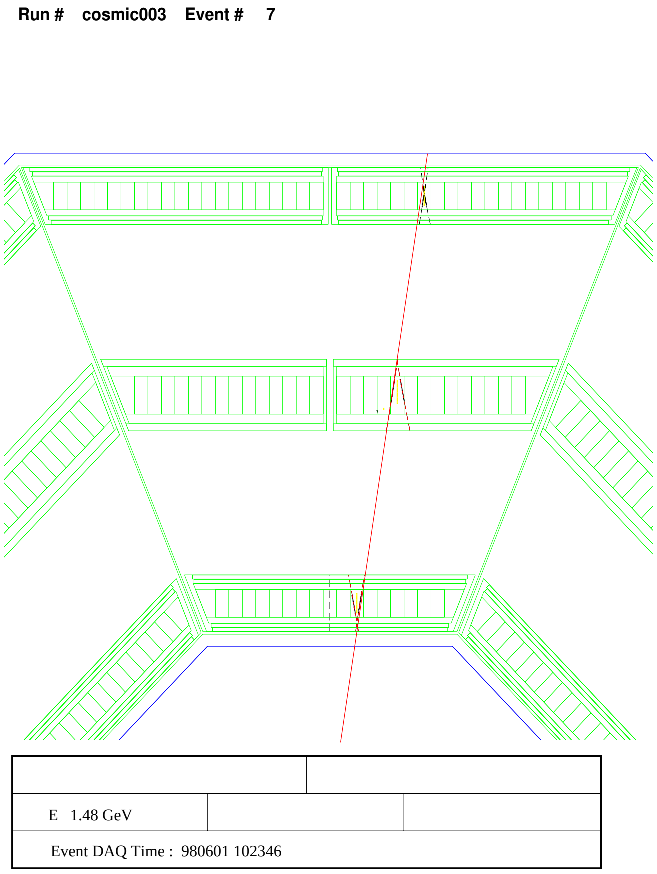

Figure 7.1: The first reconstructed event.

Chapter 8

Acknowledgement

First of all I would like to thank my supervisor Prof. Thomas Hebbeker. His questions and suggestions guided me throughout this work.

A special thanks goes to the members of the Nijmegen COL3 programming team: Albert van Mil, Bert Petersen and Henric Wilkens. Working together with them was an enjoyable experience. Despite all necessary work they never lost their sense of humour.

I'm grateful to Prof. Rudolf Leiste who answered patiently all my questions about scintillators.

I have to thank the members of the Experimental Particle Physics Working Group at Humboldt University. They provided a very convenient work environment.

I also have to mention my parents and my friends. Without their support and entertainment I would have suffered major difficulties.

Appendix A

Data cards

A.1 SIL3C

TRIG nevents Triggers a number of events.

GEOM volume parameter Specifies the volumes to be created. If the parameter is -1 the corresponding volume is not created. The default parameter is 3. There are three levels of volume keys :
1. 'LEP3'
2. 'xREG' for the 6 regions (x=T,E,H,F,M,A)
3. geometry keywords per REGion:
T region : 'TECH', 'TRBP' (xxBP stands for Beam Pipe structures)
E region : 'EBAR', 'ECAP', 'ERBP'
H region : 'HBAR', 'HCAP', 'HMFL', 'SBAR', SCAP'
F region : 'FCAP', 'FRBP', 'FQUA' (FQUA for quads. geometry)
M region : 'MBAR', 'MCAP', 'MGNT' (MGNT for magnet geometry)
A region : 'TSCN'

SETS detector parameter Specifies the detector response required. There are three levels of detector keys :
1. 'LEP3'
2. detector 'SCNT', 'MUCH', 'JTRG', 'TSCN'
3. subdetector keywords :
SCNT 'SBAR', 'SCAP'
MUCH 'MBAP', 'MBAZ'
JTRG 'JTMU', 'JTSC', 'JTL2', 'JTL3'
TSCN 'T0SC'

The parameter defines the appropriate action for the detector:

0 Nothing
1 Hits only
2 Hits and digitizations (default, may be omitted)
3 Hits, digitizations and noise

PHAS setup This defines the t0 scintillator setup to be used. For PHASE 1 $48m^2$ scintillator are created, PHASE 1.5 corresponds to $72m^2$ covered. Three scintillators of $72m^2$ are installed for PHASE 2.

FLMP filename Specifies the path to the magnetic field map for the yoke and coil region. Usually `col3/db/l3_50.map` is used.

IOPA key unit [chopt recordlength filename] Defines input and output files. If unit is negative optional parameters have to be given. Avalaible keys are:

COSM	input of cosmic events in /L3CEVT/ format
	chopt has to be 'LI' (C–library open for input)
GETY	input of standard generator events
DAQC	output of the new L3+COSMICS DAQ format [54]
	chopt has to be 'AO' (ASCII open for output)
	the new format requires wiring information from muon database
	A correct DAQ time has to be specified as well
SAVX	standard SIL3C output
HSTO	histogram output
	here the list of parameters is slightly different:
	unit chopt recl maxrec filename
	chopt has to be 'RO' (open random access output)
	maxrec gives the maximum filesize in records

The parameter chopt defines open parameters:

O	open for output
I	open for input
A	open as ASCII
U	open fortran unformated
L	open with C-library (CFIO)
	this allows the use of pipes
	and CFIO input/output commands
R	open as random access file
T	is a tape file
V	file to be obtained using L3STAGE
W	file to be staged from tape (no T option please)
X	open as Binary exchange format FZ file
Z	allow overwritting'

DBL3 key unit [recl maxr chopt dopt] vers filename Defines database to use. Allowed keys are 'DBL3', 'DBMU', 'DBSC' and 'DBJT'. The database is specified by version and filename. If the unit is negative some additonal parameters have to be given. The first parameters are recordlength and maximum file size. The next two are options for file and database opening (e.g. 'R' and ' ').

DAQT yymmdd hhmmss Sets DAQ time of the event. The DAQ time is needed to access the correct database information.

CUTX parameter Kinetic energy cuts in special tracking media on (X=E,G,H,M,N) electrons, gammas, hadrons, muons and neutrons. For each medium a parameter is needed:

1	—	gas in TEC
2	—	special air
3	—	Brass
4	—	gas in HCAL/FWCH
5	—	gas in Mu-P chamber
6	—	gas in Mu-Z chamber
7	—	Uranium mixture
8	—	RPC Gas
9	—	Gas in FB Mu-chamber
10	—	Aluminium
11	—	Iron
12	—	Molasse above L3

A.2 TRACK

SMEAR T The shower axis is smeared in a circle of 140 m diameter. Without smearing the shower axis always goes through the origin.

SELECT T If SELECT is enabled particles with an extrapolated hit position outside a circle of 16 m radius around the L3 vertex are not tracked.

REUSE F REUSE smears the primary vertex again until a particle has a chance to hit the L3 volume. This option requires SMEAR and SELECT to be activated.

EVOL volkey Particles are stopped at the borders of the specified volume. The two volumes are LEP3, a cylinder of 9.5 m radius and 14.2 m length and TSCN a box of 12.35 m x 6.35 m x 0.33 m around the t0 detector position.

FINM filename The name of the input file is specified. The program can read CORSIKA files and /L3CEVT/ formats. A CORSIKA file is assumed when the filename starts with 'DAT'. The /L3CEVT/ files are recognized via the file extensions '.l3c' and '.ntp'.

FONM filename This defines the output file path.

Appendix B

Data format and Interface library

B.1 L3CEVT data format

The underlying data structure used for data interchange is based on the /L3CEVT/ common block. This structure is inspired by the HEP common [55]. The coordinate system used is the usual L3 coordinate system. The common /L3CEVT/ contains the output variables for one event:

nevl3c	event number (1,2,3,....)
nshl3c	shower number producing this event(e.g. CORSIKA event nr.)
nrul3c	run number (e.g. CORSIKA run nr.)
ndal3c	Modified Julian date (Universal Time) (50814 - ...)
timl3c	day time, fraction of a day (Universal Time) (0 ... 0.99999..) time = time of impact of primary particle on atmosphere
idpl3c	identifier of primary particle impinging on atmosphere following jetset standard, e.g. proton = 2212
ppl3c(4)	4 momentum of primary particle: ppl3c(1) = x momentum component = px/ptot (-1 ... 1) ppl3c(2) = y momentum component = py/ptot (-1 ... 1) ppl3c(3) = z momentum component = pz/ptot (-1 ... 1) ppl3c(4) = energy in GeV
vpl3c(4)	impact point/time of primary particle (in upper atmosphere): vpl3c(1) = x coordinate in m vpl3c(2) = y coordinate in m vpl3c(3) = z coordinate in m vpl3c(4) = time difference of impact with respect to timl3c in s (normally 0 !)
nl3c	number of secondaries arriving at surface of earth
ipl3c(nl3c)	identifier of secondary particle following jetset standard (muon = 13, antimuon = -13)

pl3c(4,nl3c)	4 momentum of secondary particle: pl3c(1) = x momentum component = px/ptot (-1 ... 1) pl3c(2) = y momentum component = py/ptot (-1 ... 1) pl3c(3) = z momentum component = pz/ptot (-1 ... 1) pl3c(4) = energy in GeV
vpl3c(4,nl3c)	impact point/time of secondary (surface): vl3c(1) = x coordinate in m vl3c(2) = y coordinate in m vl3c(3) = z coordinate in m vl3c(4) = time difference of impact with respect to timl3 in s

Optional it is possible to use the same common block for header information, flagged by a negative event number nevl3c. Typically there is one such block per file (e.g. at the beginning).

nevl3c	-1
ndal3c	date of generation (s. above)
timl3c	version (and revision number) of program producing file (e.g. generator, e.g. version 2.7)
idpl3c	program code: 101 = corread 202 = l3cgen 301 = track
ppl3c,	program dependent parameters
vpl3c	ditto

B.2 Interface library

For input/output the library `l3cout` is provided. This library contains a collection of routines to read and write the /L3CEVT/ structure to disk. A C–style file format based on the CFIO package of CERNLIB (Z310) is used.

Files are opened with a call to `OPENC`. The returned value for the file descriptor LUN has to be used in all other calls. As status variable IERR is returned. After succesful execution it is set to zero. Normally files are written via `WRITEL3CEVT` and read by `READL3CEVT`. To read the compressed MINI format optionally written by L3CGEN the routine `READL3M` has to be called. As an option the information is read from integer variables INT1 and INT2 and not from a file, if LUN is zero.

Routines in `l3cout`

```
OPENC(LUN,FNAME,IERR)          - open file
WRITEL3CEVT(LUN,IERR)          - write common /L3CEVT/ to file
READL3CEVT(LUN,IERR)           - read common /L3CEVT/ from file
READL3M(LUN,INT1,INT2,IERR)    - read common /L3CEVT/ from file
                                 in L3CGEN miniformat or integer
PUTWORD(LUN,WORD,IERR)         - C-style putword
```

```
WRITEREAL(LUN,RWORD,IERR)       - writes a real to file
WRITEINT(LUN,IWORD,IERR)        - writes an integer to file
GETWORD(LUN,WORD,IERR)          - C-style getword
READREAL(LUN,RWORD,IERR)        - reads a real from file
READINT(LUN,IWORD,IERR)         - reads an integer from file
```

Appendix C

SIL3C Output

C.1 DAQ format

With the IOPA option DAQC the new L3+Cosmics DAQ event format can be written [54]. As this format needs wiring information from the database a valid time DAQT has to be specified. The output is exactly the same as for a real DAQ event. But in addition a Monte Carlo Block is written:

<table>
<tr><th>Description</th><th>31...28</th><th>27...24</th><th>23...20</th><th>19...0</th><th>Type</th></tr>
<tr><td>$\ddots$
Filter output</td><td>$\ddots$</td><td>$\ddots$</td><td>$\ddots$</td><td>$\ddots$</td><td>$\ddots$</td></tr>
<tr><td>Begin of MCB</td><td>0000</td><td>1101</td><td>0000</td><td>MCB WCNT</td><td>Integer</td></tr>
<tr><td>MCB</td><td colspan="2">primary ID(16bit)</td><td colspan="2">Number of particles to follow (16bit)</td><td>Integer</td></tr>
<tr><td>MCB</td><td colspan="2">azimuth (0.1 mrad)</td><td colspan="2">zenith (0.1 mrad)</td><td>Integer</td></tr>
<tr><td>MCB</td><td colspan="4">primary energy in GeV</td><td>Real</td></tr>
<tr><td>Begin of MCB subblock</td><td>0000</td><td>1110</td><td>0000</td><td>MCB WCNT</td><td>Integer</td></tr>
<tr><td>MCB particle subblocks</td><td>particle ID(8 bit)</td><td colspan="3">particle Energy in MeV (24bit)</td><td>Integer</td></tr>
<tr><td>MCB particle subblocks</td><td colspan="2">azimuth (0.1 mrad)</td><td colspan="2">zenith (0.1 mrad)</td><td>Integer</td></tr>
<tr><td>MCB particle subblocks</td><td colspan="4">X global in cm</td><td>Real</td></tr>
<tr><td>MCB particle subblocks</td><td colspan="4">Y global in cm</td><td>Real</td></tr>
<tr><td>MCB particle subblocks</td><td colspan="4">Z global in cm</td><td>Real</td></tr>
<tr><td>End of event</td><td>0000</td><td>1000</td><td>0000</td><td>Event WCNT</td><td>Integer</td></tr>
</table>

Figure C.1: Structure of one Event

Appendix D

SIL3C flow chart

D.1 data cards

—UGINIT		user initialization routine for GEANT3-L3C simulation
—SIDATA		define datacards via calls
		⋮
—SIDATM	foreseen for specific muon	⋮
—SIDATS	scintillator	to FFKEY
—SIDATT	t0 and	⋮
—SIDATU	user data cards	of the FFREAD
—JTSDAT	trigger cards	⋮
		⋮
		⋮
—UTDATA		package
—UTDIN		
—FFGO		read datacards
—UTRUID		interpret
—UTLLST		given
—UTMLST		data
—UTIDAD		cards
—UTIOPA	input-output	

```
| | | —UTSELE
| | | —UTJBKP
| | | —UTBRUN
```

D.2 input/output

```
|—UTIOPA                                         decode
|   |—UTIOPM                                     IOPA card
|   |—UTIOPD   decode parameters                 open files
|   |          for each unit in IOPA
|   |
|   |—UTFOPN   open files                        and mount tapes
```

Important variables:

NLUNL3		number of used units
LUNSL3()		array equivalent to each unit (e.g. L3DEBU=LUNSL3(1))
CMODE()		default open option
NRECS()		default reclength
CUNIT()		unit names
IACTS()		required open action
	1	FZ init via UTGOPN
	2	hbook file init via HRFILE
	100	FZ file init via FDFILE instead of FZFILE
	1000	suppress abortion on errors for this unit
	10000	use DAD list for input if given
KACTS()		reopen action in REL
LPTRUI()		c-file handle if open with chopt=L

D.3 hit and digi structure

```
|—UGINIT                        user initialization routine
|   |                           for GEANT3-L3C simulation
|   |
|   |—UTJSET                    define sensitive
```

```
|    |  —SIJSET                     volumes via GSDET
|    |
|    |  —UTSETI                     fill pointers,
|    |  —UTSETS                     set and volume
|    |                              arays
|    |  —SISETH                     define subdetector
|    |     |                        hits via GSDETH
|    |     |  —SISHIN    SBAR
|    |     |  —SIMHIN    MUCH
|    |     |  —SITHIN    T0SC
|    |
|    |  —UTSETH                     define main
|    |     |                        hits via GSDETH
|    |     |  —UTSHIN
|    |     |  —UTMHIN
|    |     |  —UTAHIN
|    |
|    |  —SISETD                     fill detector pointers
|    |     |
|    |     |  —SISDIN    SBAR
|    |     |  —SIMDIN    MUCH
|    |     |  —SITDIN    t0
|    |     |  —JTSINI    trigger
|    |
|    |  —UTSETD                     define digis
|    |     |                        via GSDETD
|    |     |  —UTSJDI
|    |     |  —UTMJDI
|    |     |  —UTAJDI
|    |
|    |  —SIDETH                     drop temp hits
```

Important variables:

IxxSUA	Position index of sensitive detector in GEANT list ISET
LSET	complete list of sets (e.g.MUCH)
LDET	complete list of detectors (e.g.MBAR)
LSETUA	list of current sets
LDETUA	list of current detectors
MSETUA	key word argument (e.g. hits,digi,noise)
MDETUA	key word argument (e.g. hits,digi,noise)
IACTUA	required action (hits, digi,noise)

D.4 tracking

```
|—QNEXTE                                        event loop
|  |
|  |—GUKINE                                     get kinematics
|  |
|  |—GUTREV
|  |  |
|  |  |—GTREVE
|  |     |
|  |     |—GUTRAK
|  |     |  |
|  |     |  |—GTRACK
|  |     |     |
|  |     |     |—GUSTEP                         tracking step
|  |     |        |                             record
|  |     |        |—SISHIT                      parameters
|  |     |        |—SIMHIT                      of hits after
|  |     |        |—SIT0HIT                     each step
|  |     |
|  |     |—SISAHX                               rearrange hits
|  |     |—SIMAHX                               from subdetectors
|  |     |—SIT0AHX                              into main sets
|  |
|  |—GUDIGI                                     perform digitisations
|  |—GUOUT
|  |
|  |—GTRIGC                                     clear stack
```

Important variables:
GEANT commons /GCTRAK/, /GCVOLU/, /GCSETS/ and /GCKINE/ contain detailed information for each tracking step (energy loss, particle momentum, current volume ...)

D.5 writing of DAQ format

```
|—UGINIT                                        user initialization routine
|  |                                            for GEANT-L3C-simualtion
```

—SIDBUSE	read wire map from db
—SIDBCL	close database
—WRITERUNHEAD	run header
—QNEXTE	event loop
—GUOUT	analysis and
—SISAVE	output of current event
—GETEVINFO	obtain
—WRITEEVHEAD	event header
—WRITEDAQEVENT	write hit data for each NIMROD, FElink and TDC
—WRITEEVTRAIL	event trailer
—WRITEMCB	MC info
—UGLAST	termination routine
—ZEND	
—WRITERUNTRAIL	run trailer

Appendix E

Utility programs

E.1 corread

This is a utility to read CORSIKA data. Only normal data can be read. Data from CORSIKA's thinning version have a different file format. The program `corread` takes as input parameter the CORSIKA run number and the directory path. The CORSIKA file DAT0000XX with the corresponding run number is read and an output file c0000XX is written. The output format is a ntuple with variables similar to the /L3CEVT/ common described above. As an option the /L3CEVT/ event format can be written. There exist several versions. The standard code selects only muons for output. A seperate version writes out all particles at the lowest observation level. The tiling version applies the tiling mechanism described in section 4.1.2. This version converts each CORSIKA shower into a number of events.

E.2 cors2gobi

The development of a shower can be visualized using `cors2gobi` and XGobi[56][57]. This program takes the three output files (tracksxx.em, tracksxx.mu,tracksxx.had) of CORSIKA's plot version as input. The output is compatible with the viewer XGobi. The three components are drawn in different colors. The program XGobi allows different viewing angles and zoom levels. The picture can be printed or saved as postscript. An example can be seen on the cover of this thesis.

E.3 l3cevtread

The short program `l3cevtread` converts a file written in C-style /L3CEVT/ event format into an easy to handle hbook file.

Bibliography

[1] V.F.Hess. Über Beobachtungen der durchdringenden Strahlung bei sieben Freiballonfahrten. *Phys.Zeitschr.*, (13):1084, 1912.

[2] R.A.Millikan and G.H.Cameron. High frequency rays of cosmic origin. *Phys.Rev.*, (28):851–68, 1926.

[3] W.Bothe und W.Kolhörster. Das Wesen der Höhenstrahlung. *Z.Phys.*, (56):751, 1929.

[4] D.V.Skobelzyn. Über eine Neue Art sehr schneller Beta-Strahlen. *Z.Phys.*, (54):686, 1929.

[5] C.D.Anderson. The Positive Electron. *Phys.Rev.*, (43):491, 1933.

[6] C.D.Anderson and S.H.Neddermeyer. Note on the Nature of Cosmic–Ray Particles. *Phys.Rev.*, (51):884, 1937.

[7] C.M.G.Lattes, G.P.S.Occhialini, and C.F.Powell. Observation on the Tracks of Slow Mesons in Photographic Emulsions. *Nature*, (160):453, 1947.

[8] L.Leprince-Ringuet and M.Lheritier. On the Probable Existence of Cosmic Ray Particle with Mass 990 m_e. *Compt.Ren.*, (219):618, 1944.

[9] E.Fermi. *Phys.Rev.*, (75):1169, 1949.

[10] I.S.Shklovsky. *Dokl.Akad.Nauk*, (90):983, 1953.

[11] M.Schmidt. *Nature*, (197):1040, 1963.

[12] G.E.Allen et al. Evidence of X–ray Synchrotron Emission from Electrons Accelerated to 40 TeV in the Supernova Remnat Cassiopeia A, 1997. PREPRINT: astro-ph/9707110.

[13] T.Tanimori et al. Discovery of TeV Gamma rays from SN1006:further Evidence for the SNR ORIGIN of cosmic rays, 1998. PREPRINT: astro-ph/9801275.

[14] Particle data group. Review of particle physics. *Phys.Rev.D*, 54(1), 1996.

[15] M.S.Longair. *High Energy Astrophysics*, volume 2. Cambridge University Press, 1994.

[16] C.Grupen. News from Cosmic Rays at High Energies, November,1983. Talk given at DESY, Hamburg.

[17] T. K. Gaisser. *Cosmic Rays and Particle Physics*. Cambridge University Press, Cambridge, New York, Port Chester, Melbourne, Sydney, 1990. ISBN 0 521 33931 6.

[18] J. Baehr et al. Precision Measurement of the Cosmic Ray Muon Momentum Spectrum between 20 and 2000 GeV/c, 1996. L3 internal note No. 1977.

[19] M.Aglietta. LVD Collaboration. Muon 'Depth-Intensity' Relation Measured by LVD Underground Experiment and Cosmic-Ray Muon Spectrum at Sea Level . hep-ex/9806001.

[20] Y.Fukuda. Super-Kamiokande Collaboration. Evidence for oscillation of atmospheric neutrinos. hep-ex/9807003.

[21] B.C.Rastin. *J.Phys.*, G(10):1629–38, 1984.

[22] M.Ambrosio et al. MACRO collaboration. *Phys.Rev.*, 52(7):3793, 1995.

[23] M.Ambrosio et al. Observation of the Shadowing of Cosmic Rays by the Moon using a Deep Underground Detector, 1998. hep-ex/9807006.

[24] A.Borione. *Phys. Rev.*, D(49):1171, 1994.

[25] M.Amenomori. *Phys. Rev.*, D(47):2675, 1993.

[26] O.Carrel and M.Martin. *Phys.Lett*, B(325):526, 1994.

[27] J.Kempa and A.Michalec. Interaction of Cosmic Ray Nuclei with the Sun. In *Nuclear Astrophysics HIRSCHEGG '98*, 1998. Proceedings of the Int. Workshop XXVI on Gross Properties of Nuclei and Nuclear Excitations.

[28] H.Chen et al. *Phys.Rep.*, (282):1–34, 1997.

[29] B.Adeva et al. L3 collaboration. *Nucl. Inst. Meth.*, A(289):35, 1990.

[30] A.Ball et al. Search for Cosmic Ray Coincidences with Detectors in the LEP Tunnel, 1994. LEPC 94-10.

[31] A.-S. Müller. *Nucl. Phys.*, B (Proc. Suppl.)(52B):261–263, 1997.

[32] M.Fabre. *The dimuon mass resolution of the L3 experiment at LEP*. PhD thesis, ETH–Zürich, 1992.

[33] Yue Peng. *The muon spectrometer of the L3 detector at LEP.* PhD thesis, University of Amsterdam, 1988.

[34] Albert van Mil. private communications.

[35] J.Bähr, H.-J.Grabosch, V.Kantserov, H.Leich, R.Leiste, and R.Nahnhauer. An effective method to read out large scintillator areas with precise timing, 1998. PREPRINT: physics/9801005.

[36] H.L.Groenstege and T.R.Walstra. L3 internal note 671.

[37] H.L.Groenstege, T.A.M.Wijnen, P.A.M.Reviersma, and J.Stolte. Cosmics Personality Card for the L3+Cosmics experiment. NIKHEF, May 1998.

[38] J.Christiansen. A 32 channel general purpose Time to Digital Converter. CERN/ECP-MIC.

[39] H.Verkooijen. CTT Cosmics Trigger and Timing Module. Technical Documentation. Project nr. 32010 NIKHEF, Feb 1998.

[40] B.Petersen and T.Wijnen. *L3 COSMICS Data Aquisition*, 1998. http://www.hef.kun.nl/l3c/Pub/daq.ps.

[41] B.Petersen. *L3 COSMICS online filter v1.1*, 1997. http://www.hef.kun.nl/l3c/filter/filter_man.v1.1.ps.

[42] D. Heck, J. Knapp, J.N. Capdevielle, G. Schatz, and T. Thouw. *CORSIKA: A Monte Carlo Code to simulate Extensive Air Showers.* Forschungszentrum Karlsruhe, 1998. Report FZKA 6019.

[43] G.Schatz et al. *Nucl.Phys B.*, (43):261, 1995.

[44] G.Battistoni, C. Bloise, A.Ferrari, M.Monteno, and V.Patera an d E. Scapparone. *Astroparticle Physics*, (7):101–108, 1997.

[45] T.Hebbeker and A.Korn. Simulation programs for the L3+COSMICS experiment, April,1998. L3+COSMICS internal note.

[46] Prof. R. Leiste. private communications.

[47] R. Brun et al. Geant 3. *CERN DD/EE/84-1*, september, 1987. revised.

[48] F.James and M.Roos. *MINUIT, Function Minimization and Error Analysis.* CERN. D506 Long writeup.

[49] T.Hebbeker. Moon, Sun and L3-Cosmics Experiment, January 1998. L3C internal memo.

[50] B.C.Rastin. *J.Phys.*, G(10):1609–1628, 1984.

[51] D. Heck, J. Knapp, and G. Schatz. *Comparison of Hadronic Interaction Models used in Air Shower Simulations and of their Influence on Shower Development and Observables*. Forschungszentrum Karlsruhe, 1996. Report FZKA 5828.

[52] J.A.Bakken et al. L3 BGO collaboration. *NIM*, A(343):456–462, 1994.

[53] T.V.Danilova, A.D.Erlykin, and J.Procureur. *J.Phys.*, G(15):509, 1989.

[54] B.Petersen and T.Wijnen. *L3 COSMICS Dataformat*, 1998. http://www.hef.kun.nl/l3c/Pub/data_format1_0.ps.

[55] Editors: G. Altarelli, R. Kleiss, and C. Verzegnassi. Z Physics at LEP1, 1989. CERN Yellow Report 89–08.

[56] Deborah F. Swayne, Dianne Cook, and Andreas Buja. *Users Manual for XGobi, a Dynamic Graphics Program for Data Analysis Implemented in the X Windows System*. Bellcore Technical Memorandum, 1991.

[57] Xgobi homepage: *http://lib.stat.cmu.edu/general/XGobi*.

Erklärung

Hiermit bestätige ich, daß ich die vorliegende Arbeit ohne unerlaubte fremde Hilfe angefertigt habe.

Ich bin mit der Auslage meiner Diplomarbeit in der Bibliothek der Humboldt Universität zu Berlin einverstanden.

Berlin, den 17.Juli 1998 A.Korn